Automated Multi-Sensor Data Fusion Using the Unified Data Library

Kristen Haynes[1], Jeffrey Hollon[1], Kimberly Kinateder[1], Victoria Carone[1], Tamara Payne[1], Phan Dao[1], Cory Hufford[1], Stephen Gregory[2], Scott Milster[3]

[1]Applied Optimization, [2]Stephen A. Gregory LLC, [3]AFRL/RVSW

ABSTRACT

With the development of the Unified Data Library (UDL), large amounts of commercial electro-optical data have become available for analysis. These data are collected by multiple ground-based sensors spread across the Earth and provided by multiple commercial sources. As a result, highly diversified multi-sensor data may be available for a particular satellite on any given date. Ideally, data from all the sensors collected on a satellite would be used for non-resolved object characterization, tracking, change detection, and other critical tasks of space domain awareness. However, blindly combining data from multiple sensors can result in merging different noise profiles or multiple overlapping, yet different, trends in the signature as a result of different viewing geometries, observation conditions, and data processing methods potentially used by different sensors. A signature is defined as the brightness, measured as magnitude, of a satellite as a function of the Longitudinal Phase Angle (LPA). Since noise or multiple trends in the signature can cause issues in characterizing the satellite, data from different sensors must either be kept separate or combined in a more selective manner so as to not send algorithms potentially conflicting data. While separating data from each sensor into their own separate signatures is an easy option, the resulting signatures may be too sparse in number of observations or phase angle span to use for effective analyses. Therefore, we explored methods to handle multi-sensor data that would combine subsets of the data to avoid both the issue of noisy, multi-trend signatures from all available sensors and the issue of signatures from separate sensors being too sparse for use in characterization.

This paper presents a method we developed to selectively combine subsets of data by analyzing the mathematical similarity of data trends between sensors that make up a signature in combination with the physical distance between sensor pairs. The similarity of data trends from sensor pairs is analyzed by fitting simple statistical models to each sensor independently and then to the union of each sensor pair's data. The residuals of each fit are then compared to determine if fusion of the multi-sensor data is possible. If the residuals from the fits to the individual sensors' data are considered similar to the residuals for the fit to the union of the sensors' data, then we consider the two sensors' trends to be similar and eligible for fusion. This process is performed iteratively across all possible pairs of sensors present in the data until the statistical tests indicate no more fusion may occur. Before a sensor pair's data can be fused, we also consider the geographic distance between the sensors to help guide the statistical fusion method.

Since different facets and payloads of a satellite may be visible for sensors separated geographically from one another, we leveraged simulations that considered both north-south and east-west differences in sensor locations when observing the same satellite. These simulations were used to analyze the effects of directional differences between sensors on the resulting signatures. This study aided in the determination of when the distance between sensors causes their signatures to no longer have visually similar trends. With the simulation results, we determined distance thresholds that restrict certain pairs of sensors being fused if their distance surpasses the threshold.

If a sensor pair has similar signature trends and a sufficiently small distance, the data from those sensors are fused. This process is performed iteratively until either all sensors are fused together or no remaining sensors fulfill both the trend similarity and distance requirements. The result of this process is one or more sub-signatures that can then be used for enhanced object characterization, monitoring, and change detection procedures. This paper will present the statistical method used to analyze trends in multi-sensor signatures, the simulations used to determine a distance threshold, and results of our sensor fusion method.

1. INTRODUCTION

The Unified Data Library (UDL) provides a large set of commercial electro-optical data that can be used to test methods of change detection and non-resolved object characterization [1] [2]. However, this large set of data is

challenging, as it contains a highly dynamic set of sensors that have differences in their calibrations and physical locations—causing changes in viewing geometries. Sensor biases cannot be ignored and must be properly accounted for in order to achieve optimal results for characterization and change detection algorithms while utilizing as much data for a particular satellite as possible. This paper presents a method we developed to selectively combine subsets of sensors by analyzing the mathematical similarity of data trends between sensors in combination with the physical distance between sensor pairs.

2. BACKGROUND

Since its development, the UDL has become a large database for commercial data. In particular, there is a large set of electro-optical data available for satellites in or near Geosynchronous Earth Orbit (GEO). The UDL data we have primarily studied come from one commercial data provider: ExoAnalytic Solutions. This data provider has ground-based sensors spread across the globe as do other providers. As a result of global coverage, there are many nights where the same satellite may be observed by multiple sensors. Ideally, we would use all the data for a satellite on a given night to help perform characterization or change detection on the satellite. However, as a result of these sensors being located in different regions of the world, sensors at different locations may be viewing different sides of the target satellite. These different viewing angles can result in significantly different trends in the observed signature of a satellite from sensors at different locations. A signature is defined as the brightness, measured as magnitude, of a satellite as a function of the Longitudinal Phase Angle (LPA)[1]. In addition to the location of a sensor affecting the signature, each sensor may be calibrated differently. Differences in calibrations may also result in differences between signatures taken by multiple sensors even if the sensors are located in similar geographic regions.

Since we do not know how sensors were calibrated for the data available through the UDL, we based our method for sensor fusion on the visual trends of the data measured statistically and the locations of the sensors. If the trends from two different sensors are dissimilar, we would not want to fuse those sensors' data. However, with so many satellites in orbit, a visual comparison cannot be performed manually for each satellite each night without expending an unreasonable amount of time or effort. The algorithm we propose would perform a comparison of the signatures' trends in an automated fashion while also taking into account the sensors' locations.

All data used in the development and analysis of our algorithm comes from the UDL. In particular, only data collected between October 2018 and December 2019 from ExoAnalytic Solutions was used for the research presented in this paper. This is because ExoAnalytic Solutions provided the information required to calculate LPA, needed for our analysis, while outside information is required to be added to observation data from other providers that we had access to.

3. TEST FOR SIMILAR OBSERVATION TRENDS

First, details of the statistical method used to analyze trends in multi-sensor signatures will be given. This method is used to determine which sensors' data are appropriate to fuse from a statistical point of view. Our approach to combining data from different sensors is to fit a common model (e.g., a quadratic model) to combined pairs of sensor data and analyze each pair to determine whether or not the combined data appears to statistically follow the same trend as the individual sensor's datasets. One way to see if the combined model is similar to that of the individual ones is to consider if the residuals of a fitted mean applied to the combined data have the same distribution as the residuals from the individual fits to data from each sensor. This test of residual similarity can be performed using the two-sample Kolmogorov-Smirnov (KS) test on the sets of residuals [3]. The KS test is a well-known statistical hypothesis test to test for a significant difference in the distribution of two samples.

3.1 INITIAL SENSOR FUSION METHOD

Consider a signature with observations from multiple sensors. Using a fixed model, in this case a quadratic polynomial, the following procedure is proposed to determine if data from sensor i may be combined with data from sensor j. Let the observations belonging to sensor i be denoted by S_i, i.e., S_i contains all ordered pairs of observations (magnitude and LPA) that belong to the i^{th} sensor for a given night of observations. Our initial sensor fusion method does not take into account the distance between sensors.

[1] The signed angle that represents the east-west component of the total phase angle.

For all possible pairs of sensor data in the current signature (i^{th} and j^{th} sensors) and a quadratic model:

1. Fit the quadratic model to the datasets S_i and S_j independently.
2. Calculate the corresponding sets of residuals, R_i and R_j.
3. Fit the model to the combined data $S_{ij} = S_i \cup S_j$.
4. Find the residuals for the combined fit R_{ij}.
5. Run the two-sample KS test on $R_i \cup R_j$ and R_{ij}. Report the test's p-value for all sensor pairs.
6. Find the largest p-value among all combinations of i and j that is above a user-defined threshold. Denote the pair with the highest p-value as i^* and j^*. This highest p-value indicates that $R_{i^*} \cup R_{j^*}$ comes from the same distribution as $R_{i^*j^*}$ (a large p-value indicates a lack of significant difference).
7. Merge the data in S_{i^*} and S_{j^*}.
8. Repeat steps (1) through (7) until the sensors cannot be grouped further.

Once these steps are complete, the grouped sensors from the original signature now form sub-signatures that may be analyzed by characterization or change detection algorithms. Each sub-signature represents a union of sensors on a particular night and as such there may be multiple sub-signatures for a given night's observations. The process is repeated for previously grouped sub-signatures that contain multiple sensors; however, a single model is used with sub-signatures containing multiple sensors' data. That is, previously grouped sensors are considered a single sensor from the perspective of the fusion process.

3.2 EXAMPLE

To provide further insight into this procedure, details of the process are presented to show the intermediate steps that take place for the sensor data shown in Fig. 1. This signature was taken from satellite 25933 on 2019-10-23 and is composed of five different ExoAnalytic Solutions sensors (1021, 1130, 1157, 1272, and 7006) located in four distinct regions. Each observation is colored by its sensor number. The region where a sensor is located will be indicated using the International Organization for Standardization (ISO) abbreviations (e.g., US-CA is the ISO abbreviation for California, United States of America). Sensors 1021 and 7006 are located in AU-VIC, sensor 1130 is located in US-CA, sensor 1157 is located in US-NM, and sensor 1272 is located in AU-NSW. Visual inspection reveals that likely two major trends in the data exist, the first being the sensors from Australia (1021, 1272, and 7006) and the second from the United States-based sensors (1130 and 1157).

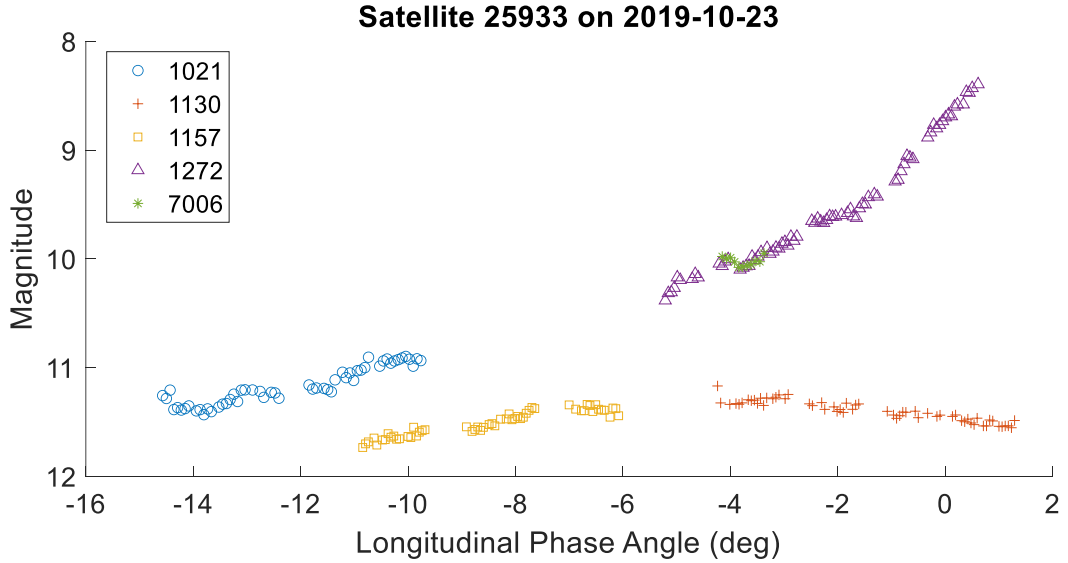

Fig. 1. Signature from Satellite 25933 Taken on 2019-10-23 Where Observations Are Labeled by Sensor

For the first iteration of the algorithm, there are five different sensors contributing data, so $\binom{5}{2} = 10$ pairs of models must be fit by the quadratic function, and their residuals must be analyzed. The sensors 1021, 1130, 1157, 1272, and 7006 are assigned numbers 1-5 respectively in the following plots. For any two of the sensors to be grouped, the p-

value reported on residuals from the KS test must be at least $\alpha = 1 \times 10^{-5}$. This level of significance, α, was chosen empirically as the resulting sensor combinations met our expectations based on the data's visual inspection and knowledge of the sensors' locations.

Analysis of two of 10 possible cases for the first run are shown in Fig. 2 and Fig. 3. The first case we examine is the sensor grouping $(i, j) = (2,3)$ shown in Fig. 2. Quadratic models were fit to the green and light blue observations individually, and then a quadratic model was fit to the combined set of green and light blue observations. The three sets of residuals are shown in the histogram in the bottom of Fig. 2. Based on visual inspection of the histogram, it appears that all of the residuals are highly similar. This indicates a reasonable grouping of the data associated with the two lower curves. The KS test reports a p-value of 0.93 that is well above our threshold of $\alpha = 1 \times 10^{-5}$.

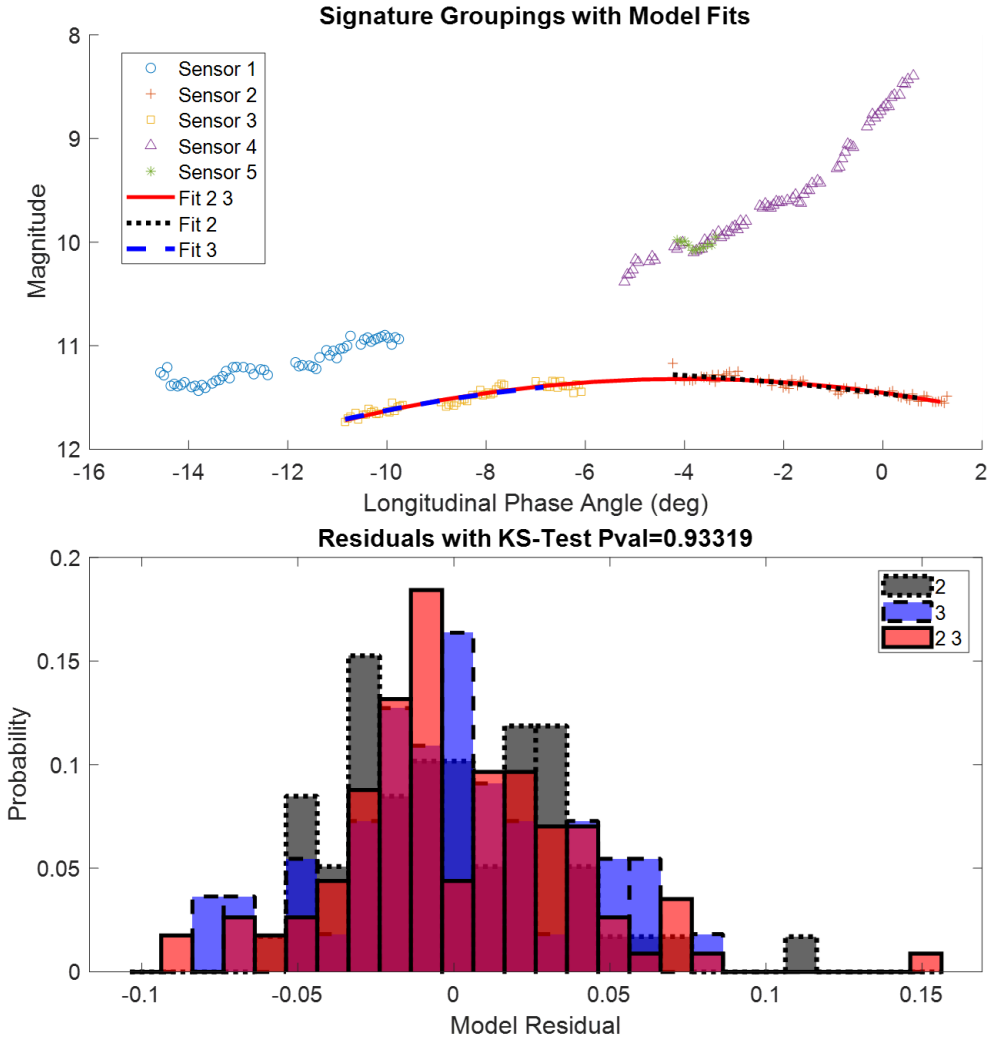

Fig. 2. Signature from Satellite 25933 on 2019-10-23. (Top) Grouping Attempt for Sensor Groups 2 and 3. (Bottom) Residuals from Fits Showing Compatible Residuals.

The second case we examine is the sensor grouping $(i, j) = (1,3)$ shown in Fig. 3. Quadratic models were fit to the green and dark blue observations individually, and then a quadratic model was fit to the combined set of green and dark blue observations. The three sets of residuals are shown in the histogram at the bottom of Fig. 3. Based on visual inspection of the histogram, it appears that all of the residuals are highly dissimilar. This indicates an unreasonable grouping of data associated with the two curves on the left. The KS test reports a p-value of 4.42×10^{-6} that is below our threshold of $\alpha = 1 \times 10^{-5}$.

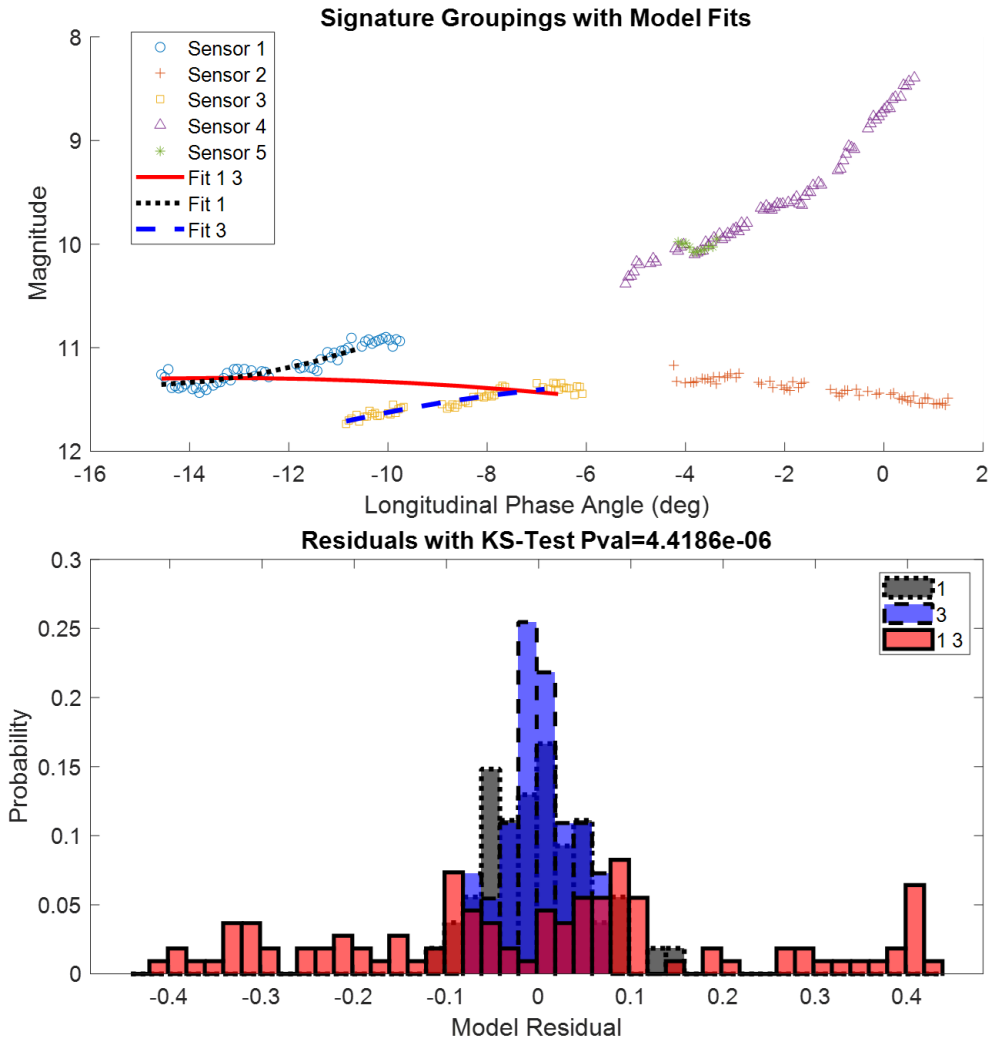

Fig. 3. Signature from Satellite 25933 on 2019-10-23. (Top) Grouping Attempt for Sensor Groups 1 and 3. (Bottom) Residuals from Fits Showing Incompatible Residuals

For brevity, the p-values of the remaining combinations are reported in Table 1. The highest value is associated with sensor grouping $(4,5)$, so those two sensors will be combined before running the algorithm again.

Table 1. For Signature from Satellite 25933 on 2019-10-23, Reported p-values from KS Test Based on Sensor Groupings from Iteration 1

Grouping Pair	$(\mathbf{1,2})$	$(\mathbf{1,3})$	$(\mathbf{1,4})$	$(\mathbf{1,5})$	$(\mathbf{2,3})$	$(\mathbf{2,4})$	$(\mathbf{2,5})$	$(\mathbf{3,4})$	$(\mathbf{3,5})$	$(\mathbf{4,5})$
KS Test p-value	1.7×10^{-4}	4.4×10^{-6}	5.5×10^{-4}	0.82	0.93	3.0×10^{-19}	1.6×10^{-5}	6.0×10^{-6}	9.7×10^{-5}	0.98

After combining sensors 4 and 5 together (they now become the label 4), we are left with four groupings to analyze pairwise. This results in $\binom{4}{2} = 6$ pairwise tests to run. The p-values for these six pairwise KS tests are in Table 2. The values indicate that sensor groups 2 and 3 may be combined (to be labeled as group 2).

Table 2. For Signature from Satellite 25933 on 2019-10-23, Reported p-values from KS Test Based on Sensor Groupings from Iteration 2

Grouping Pair	$(\mathbf{1},\mathbf{2})$	$(\mathbf{1},\mathbf{3})$	$(\mathbf{1},\mathbf{4})$	$(\mathbf{2},\mathbf{3})$	$(\mathbf{2},\mathbf{4})$	$(\mathbf{3},\mathbf{4})$
KS Test p-value	1.7×10^{-4}	4.4×10^{-6}	1.4×10^{-4}	0.93	2.8×10^{-23}	9.5×10^{-8}

For the third iteration of the algorithm, there are now only three sensor groupings remaining. This results in $\binom{3}{2} = 3$ pairs of tests whose p-values are given in Table 3. The sensor groupings labeled 1 and 4 have a p-value from the KS test larger than our threshold of $\alpha = 1 \times 10^{-5}$; thus, these are grouped together and labeled 1. This leaves two sensor groupings (one test) whose p-value is 3.7×10^{-23} and well below our threshold for grouping. The process ends with two groups, or sub-signatures, as shown in Fig. 4.

Table 3. For Signature from Satellite 25933 on 2019-10-23, Reported p-values from KS Test Based on Sensor Groupings from Iteration 3

Grouping Pair	$(\mathbf{1},\mathbf{2})$	$(\mathbf{1},\mathbf{4})$	$(\mathbf{2},\mathbf{4})$
KS Test p-value	8.2×10^{-7}	1.4×10^{-4}	4.5×10^{-24}

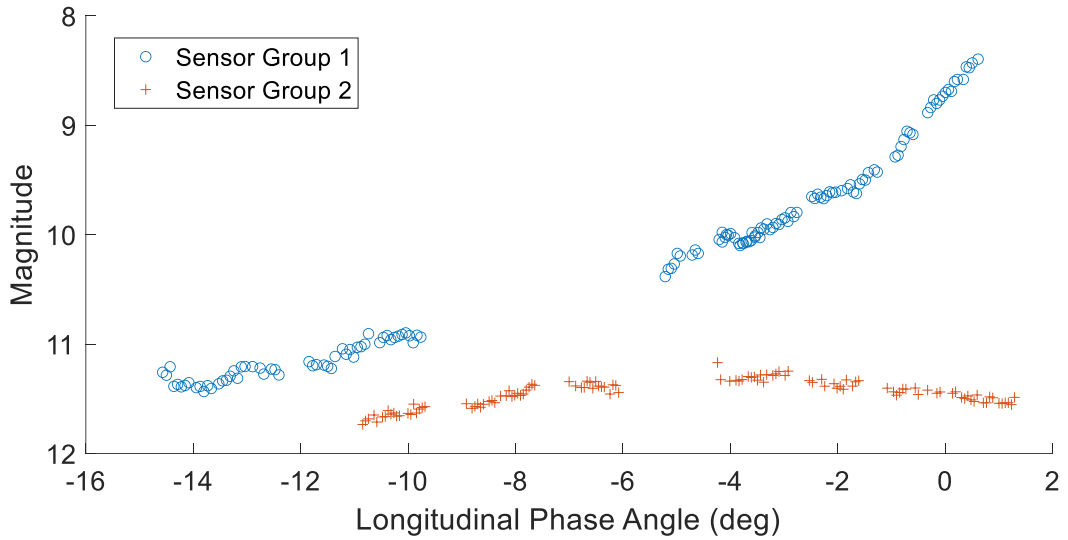

Fig. 4. Multi-sensor Data from Satellite 25933 on 2019-10-23 (Shown in Fig. 1) Grouped Based on Residuals from Fits to Pairs of Sensors

4. DISTANCE BETWEEN SENSORS STUDY

In conjunction with our sensor fusion algorithm development, we investigated how far sensors can be geographically from each other before they see significantly different portions of a satellite. This knowledge is important when determining which sensors' data can be reasonably fused as it is undesirable to fuse data from locations that are unable to physically observe similar geometries. Using a statistical method alone, it is conceivable that observations could be falsely merged especially in cases of sparse data collects when statistical tests will have little information with which to work. For this investigation, we performed Satellite Visualization and Signature Tool (SVST) simulations for sensors at various set locations on Earth [4]. We tested the effect of two types of location differences by placing sensors (1) at the same latitude and altitude but at different longitudes to test east-west differences between sensors and (2) at the same longitude and altitude but at different latitudes to test north-south differences between sensors. A Galaxy 14 model placed in an equatorial GEO in the -119° longitude slot was used as the target for all simulations.

4.1 SIGNIFICANT DISTANCE METRIC

In order to determine a threshold on the distance sensors can be and still see a similar view of the satellite, a distance metric was established to compare signatures from a pair of sensors. We compared the simulated signatures using the 90th percentile of the absolute magnitude differences between a signature pair. To compensate for the different samplings of the LPA range between sensors, we modeled the signature means using cubic splines and only calculated magnitude differences where the two signatures' LPA ranges overlapped. The algorithm used to calculate the 90th percentile of the absolute magnitude differences is as follows:

1. Range-normalize simulated magnitudes using a standard range of R=36,000 km.
2. Fit splines by ordinary least squares to the signatures from sensors A and B independently.
3. Calculate the absolute difference between each observation from site A and the spline fit for site B. Get n differences, where n is the number of points in the signature from site A that fall within the common LPA range.
4. Calculate the absolute difference between each observation from site B and the spline fit for site A. Get m differences, where m is the number of points in the signature from site B that fall within the common LPA range.
5. Find the 90th percentile of all $n + m$ differences.

Since differences in sensors' longitude and differences in sensors' latitude have different effects on a satellite's signature, the 90th percentile of absolute magnitude differences were studied separately for each case in order to arrive at a distance threshold in the east-west direction and a separate distance threshold in the north-south direction.

4.2 EAST-WEST DIFFERENCES

To test the effect of sensors with east-west differences in their locations, we placed sensors at the same latitude (20.71°) but different longitudes in our SVST simulations. Simulated signatures were created for 2019-12-05 and 2019-02-22. There were three cases we investigated:

1. Equidistant case: The two sensors (red circle and blue triangle in Fig. 5) were equidistant from the target.
2. Eastern-right-triangle case: One sensor (green square in Fig. 5) was located at the same longitude as the target, and the other sensor (blue triangle in Fig. 5) was to the east of the target.
3. Western-right-triangle case: One sensor (green square in Fig. 5) was located at the same longitude as the target, and the other sensor (red circle in Fig. 5) was to the west of the target.

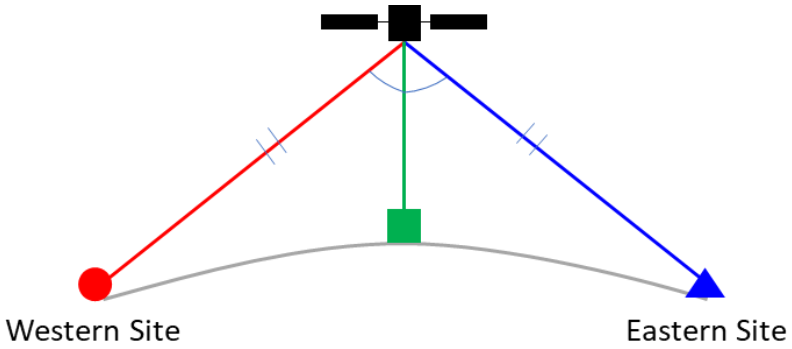

Fig. 5. Sensor Geometry with Respect to the Target for East-West Differences

Simulated signatures from three sensors with the configuration shown in Fig. 5 at varying distances are shown next. The first example shown is for three sensors with a great-circle distance of 514.28 km between the western and eastern sites; the western and eastern sites are each 257.14 km (great-circle distance) away from the central sensor. The longitudes of the three sensors are -116.69°, -119°, and -121.31°. Signatures for these sensors from 2019-12-05 and 2019-02-22 are shown in Fig. 6 and Fig. 7, respectively. The signatures from 2019-12-05 appear very similar in Fig. 6, and this similarity is reflected in the low 90th percentile of absolute magnitude differences which are 0.04 mag for the equidistant case, 0.05 mag for the eastern-right-triangle case, and 0.03 mag for the western-right-triangle

case. The signatures from 2019-02-22 shown in Fig. 7 are more noticeably different especially near the signature's peak. This difference is reflected in the slightly larger 90th percentile values for 2019-02-22 which are 0.04 mag for the equidistant case, 0.09 mag for the eastern-right-triangle case, and 0.09 mag for the western-right-triangle case.

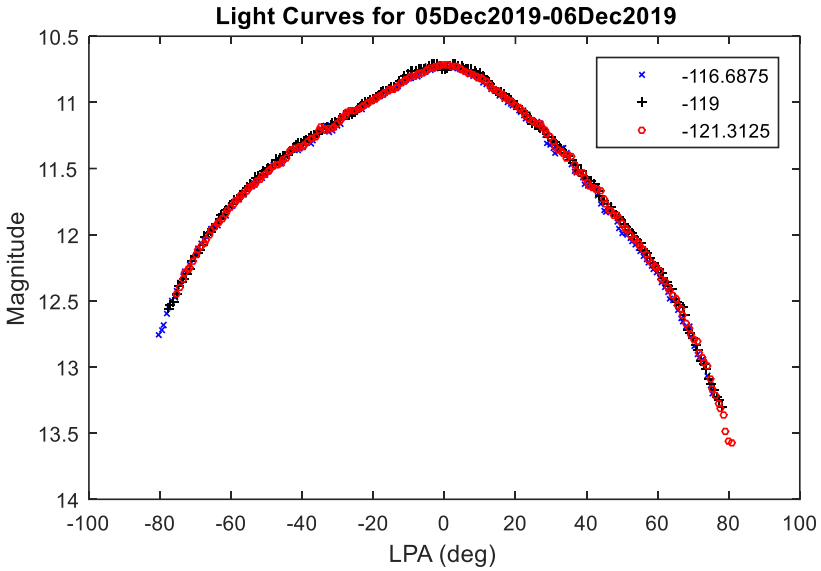

Fig. 6. Signatures from 2019-12-05 for Sensors at Longitudes -116.69°, -119°, and -121.31°

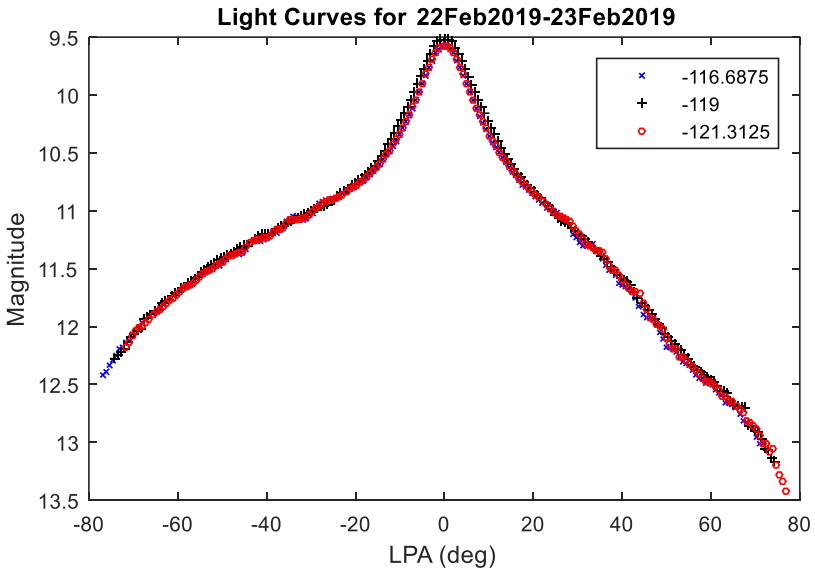

Fig. 7. Signatures from 2019-02-22 for Sensors at Longitudes -116.69°, -119°, and -121.31°

The second example shown is for three sensors with a great-circle distance of 2057.11 km between the western and eastern sites; the western and eastern sites are each 1028.55 km (great-circle distance) away from the central sensor. The longitudes of the three sensors are -109.75°, -119°, and -128.25°. Signatures for these sensors from 2019-12-05 and 2019-01-22 are shown in Fig. 8 and Fig. 9, respectively. Even at quadruple the distance of the previous example, the signatures from 2019-12-05 appear very similar in Fig. 8 though there are some slight differences on the right side of the signature. This similarity is again reflected in the low 90th percentile of absolute magnitude differences which are 0.09 mag for the equidistant case, 0.07 mag for the eastern-right-triangle case, and 0.05 mag for the western-right-triangle case. The signatures from 2019-02-22 shown in Fig. 9 are also very similar, though there are some noticeable differences on the right side of the signature like the December scenario. This difference is

reflected in the slightly larger 90th percentile values for 2019-02-22 which are 0.1 mag for the equidistant case, 0.1 mag for the eastern-right-triangle case, and 0.08 mag for the western-right-triangle case.

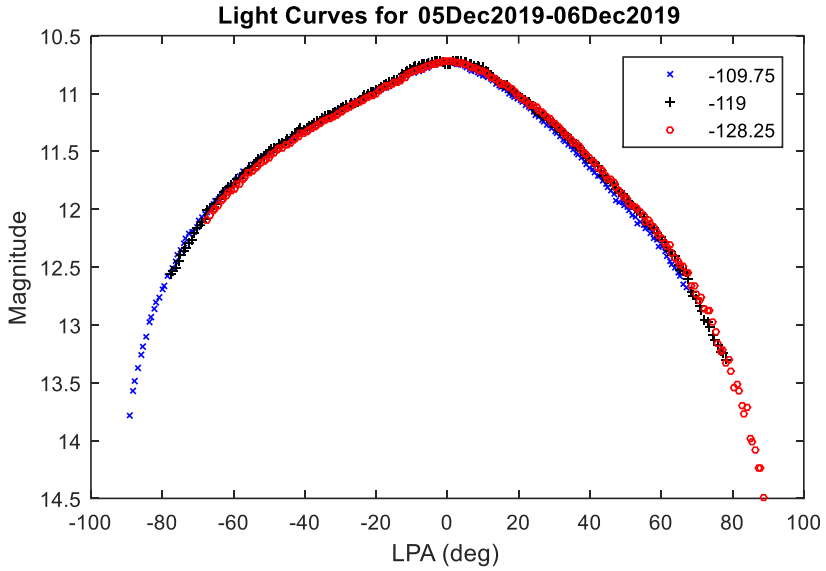

Fig. 8. Signatures from 2019-12-05 for Sensors at Longitudes -109.75°, -119°, and -128.25°

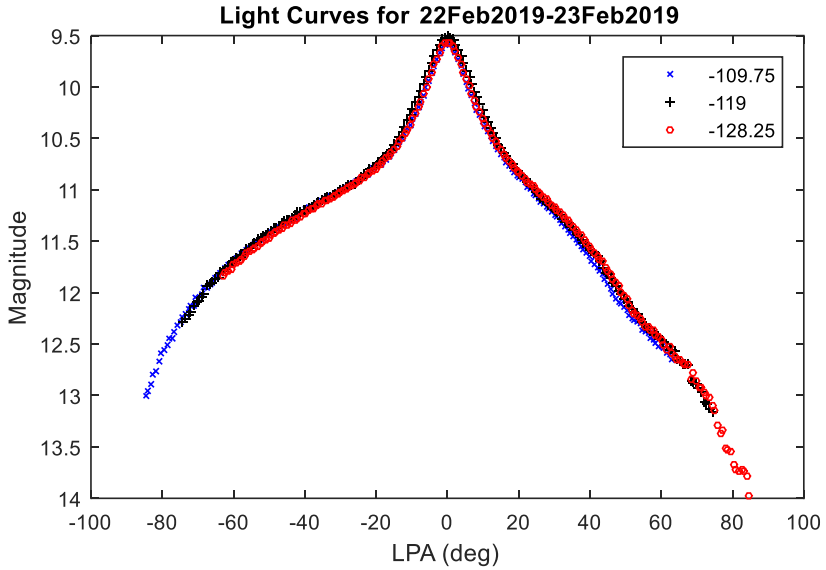

Fig. 9. Signatures from 2019-02-22 for Sensors at Longitudes -109.75°, -119°, and -128.25°

Simulations were also performed for sensors where the great-circle distance between the eastern and western sites were 1028.55 km, 4114.21 km, and 8228.42 km for the same December and February scenarios. As the east-west distance between sensors increased, differences between the signatures became more pronounced at LPA further from 0°. The 90th percentile of absolute magnitude differences for all simulations performed for sensors with different longitudes are plotted versus the great-circle distance in Fig. 10 and Fig. 11 for the December and February scenarios respectively.

To help decide a suitable cut off point for the difference in magnitude for two signatures, we analyzed the magnitude uncertainties reported for the data we used in UDL. From this analysis, we found that the minimum reported magnitude uncertainty was 0.1 magnitude. If we use 0.1 as the acceptable difference in magnitudes, then the 90th percentile of absolute magnitude differences is about 0.1 around 2000-2500 km for the December scenario and

around 1000-2000 km for the February scenario depending on whether we are looking at the equidistant, eastern-right-triangle, or western-right-triangle case. Though only the December scenario shows evidence for a distance of 2500 km resulting in a difference of magnitudes within our threshold of 0.1 mag, further analysis of real and simulated signatures provided evidence that a threshold of 2500 km would be an appropriate initial constraint for sensor fusion. Data from UDL provided examples of similar trends that would be appropriate to fuse from sensors about 2200 km apart in the east-west direction. Additionally, though there are some slight shifts in magnitude on the edges of the simulated signatures shown with east-west differences, there is no observation noise in the simulations. With observation noise, the signatures shown in Fig. 8 and Fig. 9 with a distance of over 2000 km would appear to follow the same trends. With that amount of similarity between sensor data, we deemed it appropriate to fuse those sensors for modeling the signature, object characterization, and change detection. for an initial attempt, we decided to use 2500 km as the threshold for east-west distances between sensors when fusing data from multiple sensors.

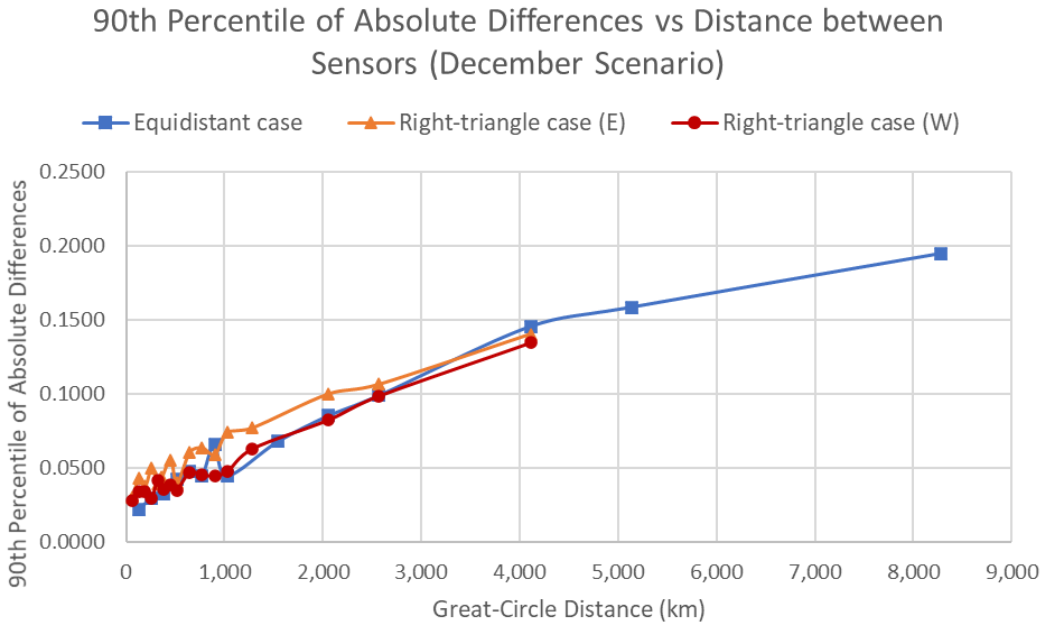

Fig. 10. 90th Percentile of Absolute Magnitude Differences versus East-West Distance (December Scenario)

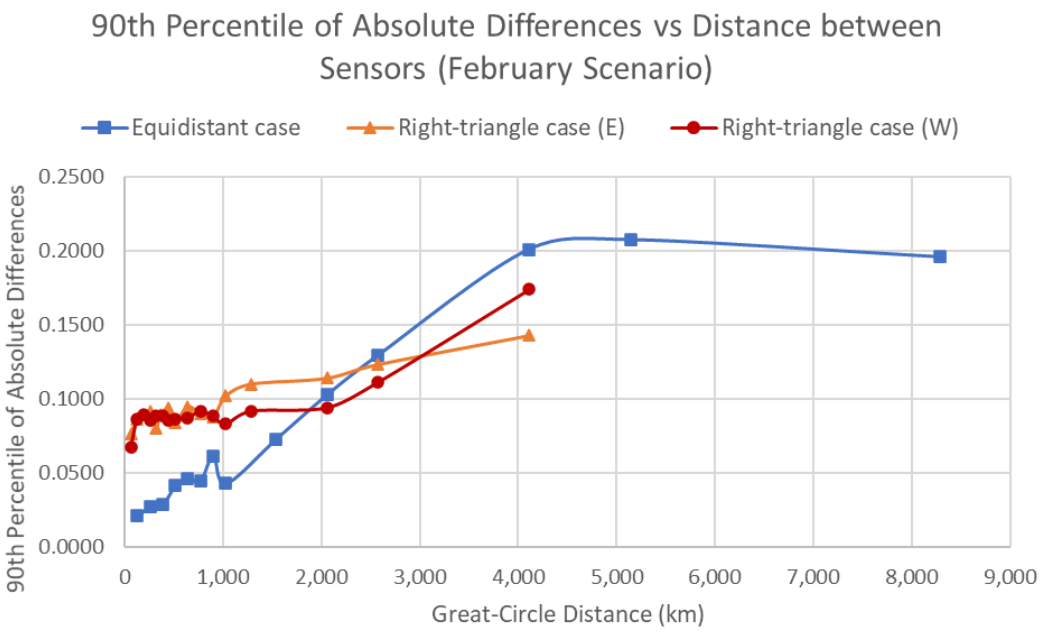

Fig. 11. 90th Percentile of Absolute Magnitude Differences versus East-West Distance (February Scenario)

4.3 NORTH-SOUTH DIFFERENCES

To test the effect of sensors with north-south differences in their locations, we placed sensors at the same longitude (-119°) but at different latitudes on three different dates: 2019-02-22, 2019-04-22, and 2019-12-05. We investigated three cases:

1. Equidistant case: Two sensors (red circle and blue triangle in Fig. 12) were equidistant from the target.
2. Northern-right-triangle case: One sensor (green square in Fig. 12) was located at the same latitude as the target, and the other sensor (blue triangle in Fig. 12) was to the north of the target.
3. Southern-right-triangle case: One sensor (green square in Fig. 12) was located at the same latitude as the target, and the other sensor (red circle in Fig. 12) was to the south of the target.

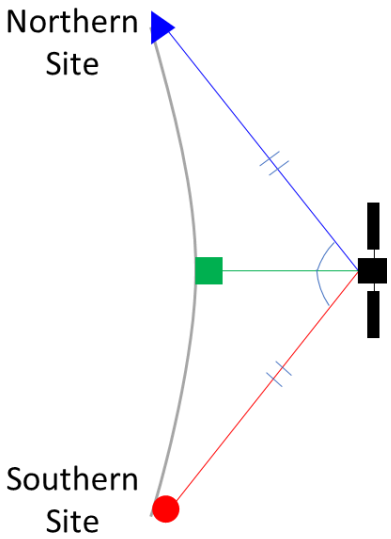

Fig. 12. Sensor Geometry with Respect to the Target for North-South Differences

Simulated signatures from three sensors with the configuration shown in Fig. 12 at varying distances are shown next. The first example shown is for three sensors with a great-circle distance of 514.28 km between the northern and southern sites; the northern and southern sites are each 257.14 km (great-circle distance) away from the central sensor. The latitudes of the three sensors are 2.31°, 0°, and -2.31°. Signatures for these sensors from 2019-12-05, 2019-02-22, and 2019-04-22 are shown in Fig. 13, Fig. 14, and Fig. 15, respectively.

The signatures from 2019-12-05 in Fig. 13 appear similar everywhere except at the peak around 0° LPA. The difference seen at the peak is much more pronounced for sensors with different latitudes, as seen in Fig. 13, compared to sensors with different longitudes, as seen in Fig. 6, even though the great-circle distance between them is the same. These differences are reflected in the slightly higher 90th percentile of absolute magnitude differences (when compared to the sensors with the same distance but in the east-west direction) which are 0.05 mag for the equidistant case, 0.05 mag for the northern-right-triangle case, and 0.05 mag for the southern-right-triangle case.

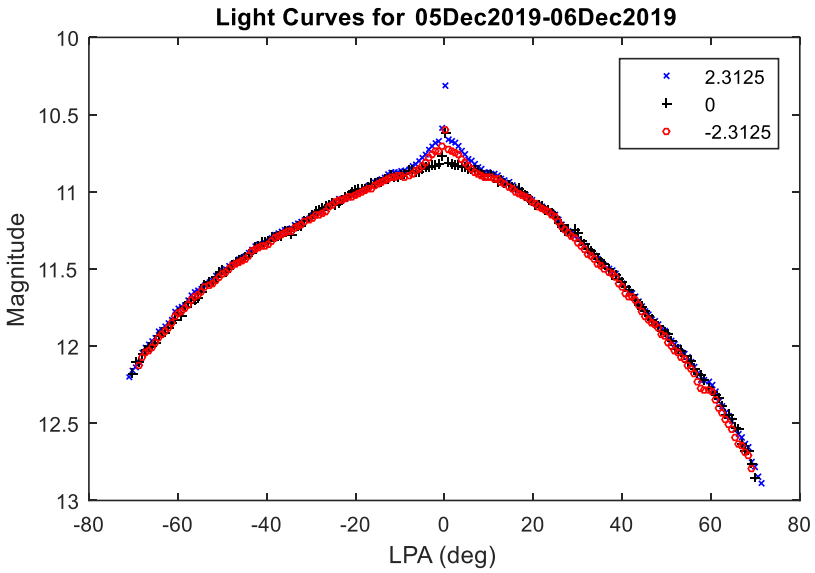

Fig. 13. Signatures from 2019-12-05 for Sensors at Latitudes 2.31°, 0°, and -2.31°

The signatures from 2019-02-22 shown in Fig. 14 are also similar everywhere except the peak where there is a noticeable difference in magnitude between the sensor at 2.31° latitude and the sensors at 0° and -2.31° latitude. The 90th percentile values for 2019-02-22 are 0.08 mag for the equidistant case, 0.05 mag for the northern-right-triangle case, and 0.06 mag for the southern-right-triangle case.

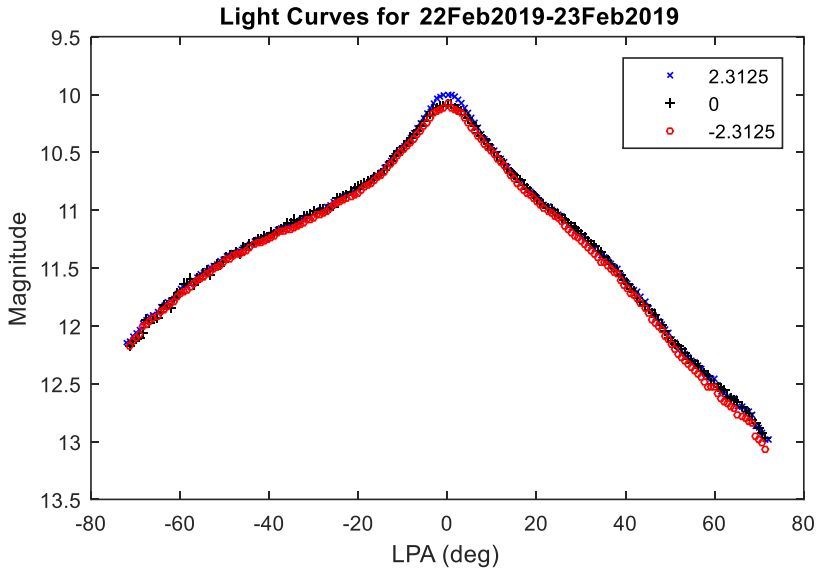

Fig. 14. Signatures from 2019-02-22 for Sensors at Latitudes 2.31°, 0°, and -2.31°

The signatures from 2019-04-22 shown in Fig. 15 are also similar everywhere except the peak where there is a noticeable difference in magnitude between the sensor at -2.31° latitude and the sensors at 0° and 2.31° latitude. The 90th percentile values for 2019-04-22 are 0.07 mag for the equidistant case, 0.05 mag for the northern-right-triangle case, and 0.08 mag for the southern-right-triangle case.

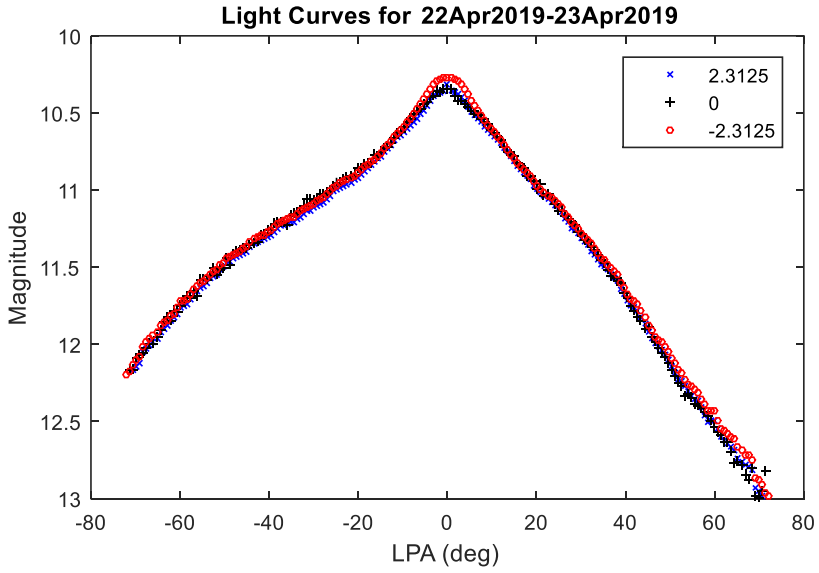

Fig. 15. Signatures from 2019-04-22 for Sensors at Latitudes 2.31°, 0°, and -2.31°

The second example shown is for three sensors with a great-circle distance of 2057.11 km between the northern and southern sites; the northern and southern sites are each 1028.55 km (great-circle distance) away from the central sensor. The latitudes of the three sensors are 9.25°, 0°, and -9.25°. Signatures for these sensors from 2019-12-05, 2019-02-22, and 2019-04-22 are shown in Fig. 16, Fig. 17, and Fig. 18, respectively.

The signatures from 2019-12-05 in Fig. 16 appear similar everywhere except at the peak around 0° LPA. The differences are again more visually pronounced for sensors with different latitudes, as seen in Fig. 16, compared to sensors with the equivalent distance but different longitudes, as seen in Fig. 8. However, the 90th percentile of absolute differences are not larger than the equivalent case for east-west differences for the December scenario. The

90th percentile of absolute magnitude differences are 0.07 mag for the equidistant case, 0.07 mag for the northern-right-triangle case, and 0.04 mag for the southern-right-triangle case.

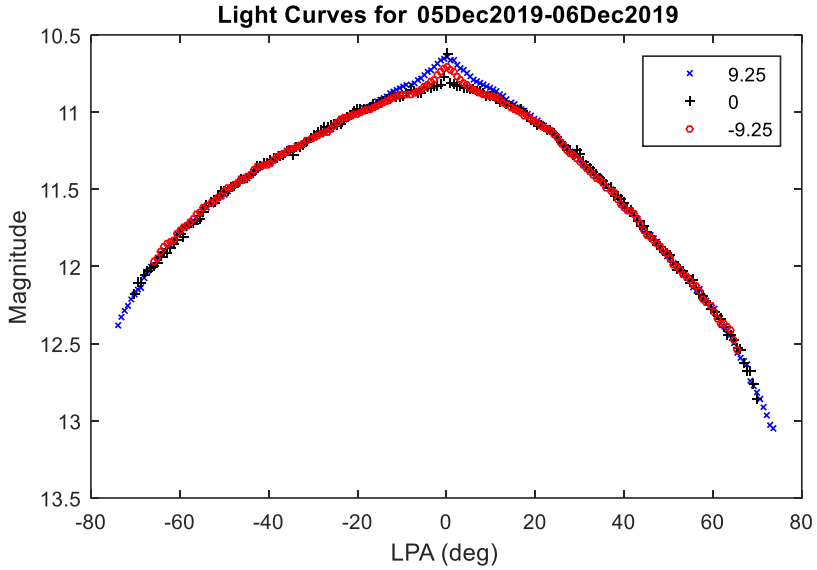

Fig. 16. Signatures from 2019-12-05 for Sensors at Latitudes 9.25°, 0°, and -9.25°

The signatures from 2019-02-22 shown in Fig. 17 are also similar everywhere except the peak where there is a noticeable difference in magnitude between all three sensors. The 90th percentile values for 2019-02-22 are 0.19 mag for the equidistant case, 0.1 mag for the northern-right-triangle case, and 0.08 mag for the southern-right-triangle case. These magnitude differences are much higher than the values for sensors with the same distance but in the east-west direction.

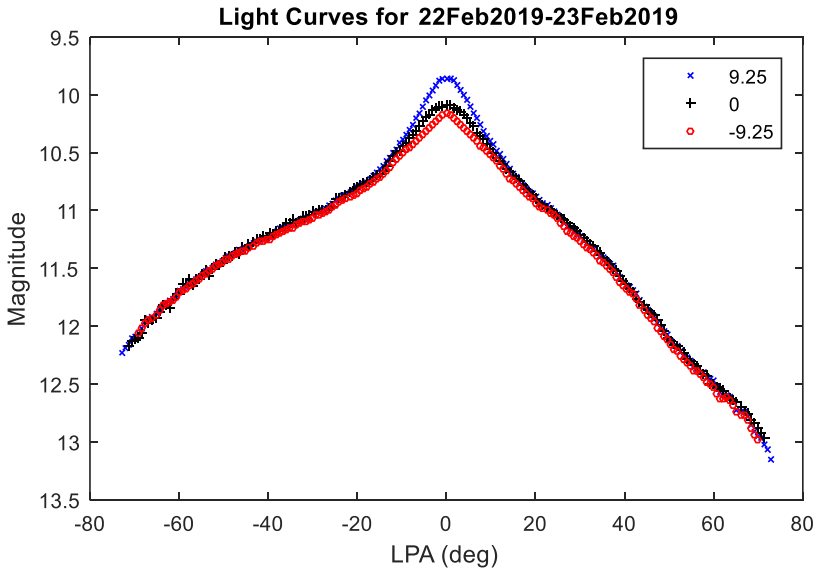

Fig. 17. Signatures from 2019-02-22 for Sensors at Latitudes 9.25°, 0°, and -9.25°

The signatures from 2019-04-22 shown in Fig. 18 are also similar everywhere except the peak where there is a noticeable difference in magnitude between all three sensors. The 90th percentile values for 2019-04-22 are 0.15 mag for the equidistant case, 0.1 mag for the northern-right-triangle case, and 0.08 mag for the southern-right-triangle case. Note that these magnitude differences are much higher than the values for sensors with the same distance but in the east-west direction.

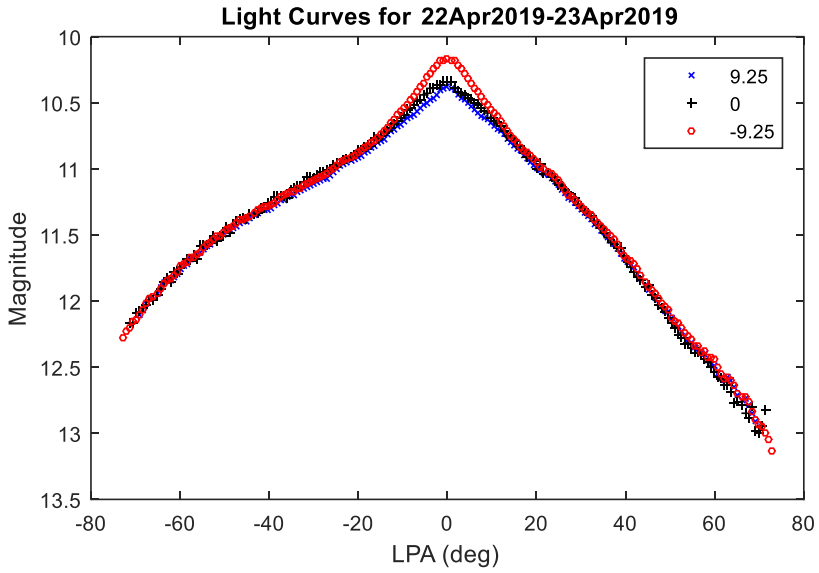

Fig. 18. Signatures from 2019-04-22 for Sensors at Latitudes 9.25°, 0°, and -9.25°

Simulations were also performed for sensors where the great-circle distance between the northern and southern sites were 1028.55 km, 4114.21 km, 6671.70 km, and 8228.42 km for the same December, February, and April scenarios. As the north-south distance between sensors increased, differences between the signatures became more pronounced at the peak near 0° LPA. The 90th percentile of absolute magnitude differences for all simulations performed for sensors with different latitudes are plotted versus the great-circle distance in Fig. 19, Fig. 20, and Fig. 21 for the December, February, and April scenarios, respectively.

To determine the distance threshold for north-south differences, we again used the minimum magnitude uncertainty reported with the data of 0.1 magnitude as the maximum acceptable difference in magnitude. The 90th percentile of absolute magnitude differences is about 0.1 mag around 4000-5000 km for the December scenario, around 500-1000 km for the February scenario, and around 500-1000 km for the April scenario depending on whether we are looking at the equidistant, eastern-right-triangle, or western-right-triangle case. The magnitude differences are very different depending on the time of year. Though we were lenient for the east-west threshold, differences in magnitude at the signatures' peaks were noticeable even when the distance between a sensor pair was just 500 km in the north-south direction. If sensors farther than 500 km apart in the north-south direction were fused, these differences may be enough to cause issues when modeling the signature or performing characterization or change detection. As a result, we decided to choose a conservative threshold of 500 km for north-south distances between sensors when fusing data from multiple sensors.

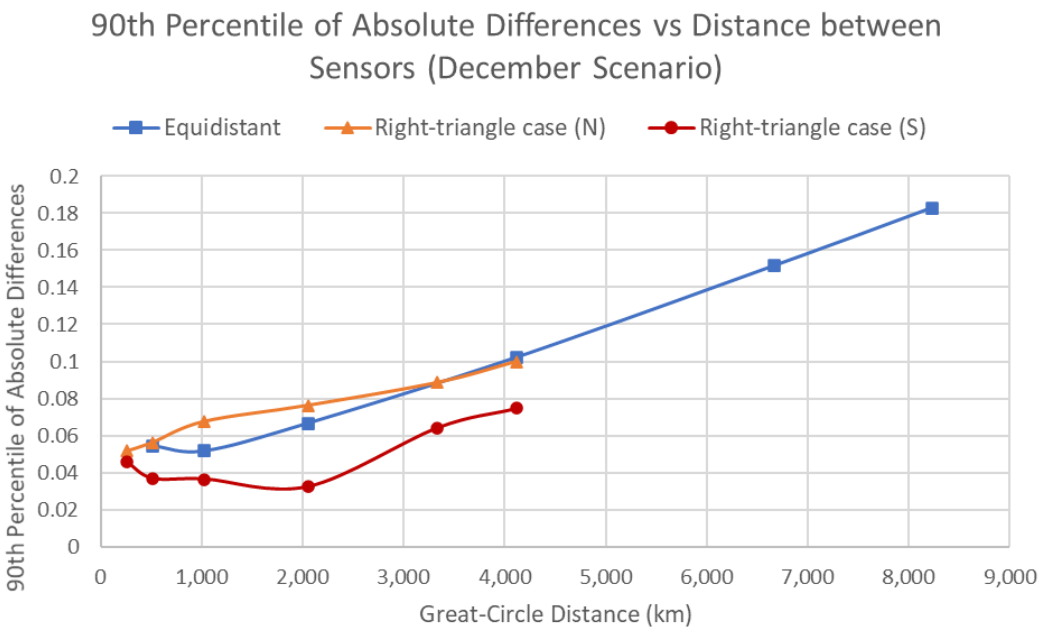

Fig. 19. 90th Percentile of Absolute Magnitude Differences versus North-South Distance (December Scenario)

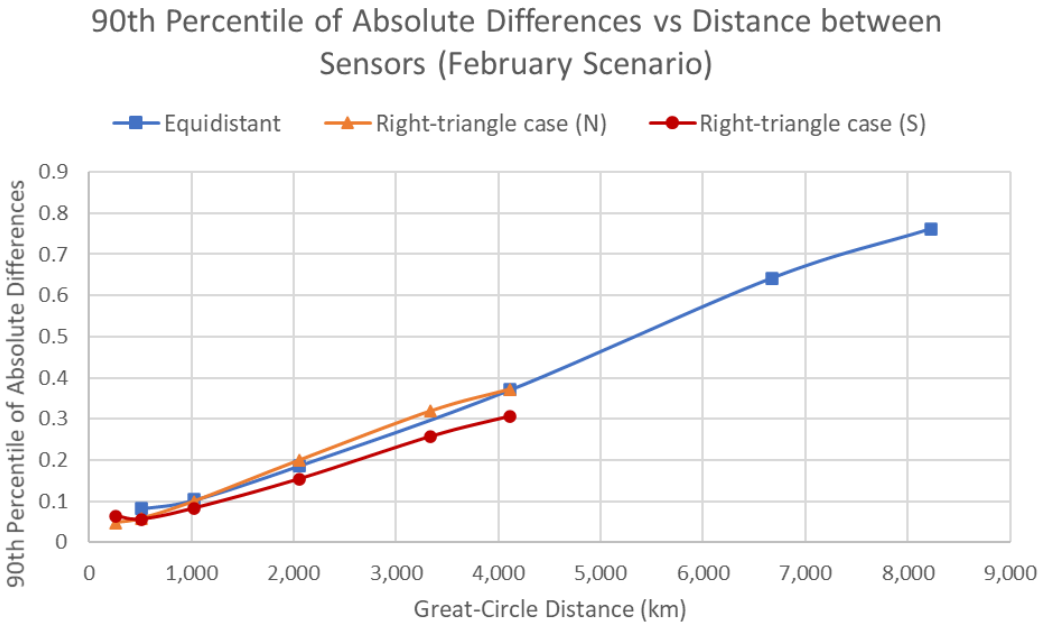

Fig. 20. 90th Percentile of Absolute Magnitude Differences versus North-South Distance (February Scenario)

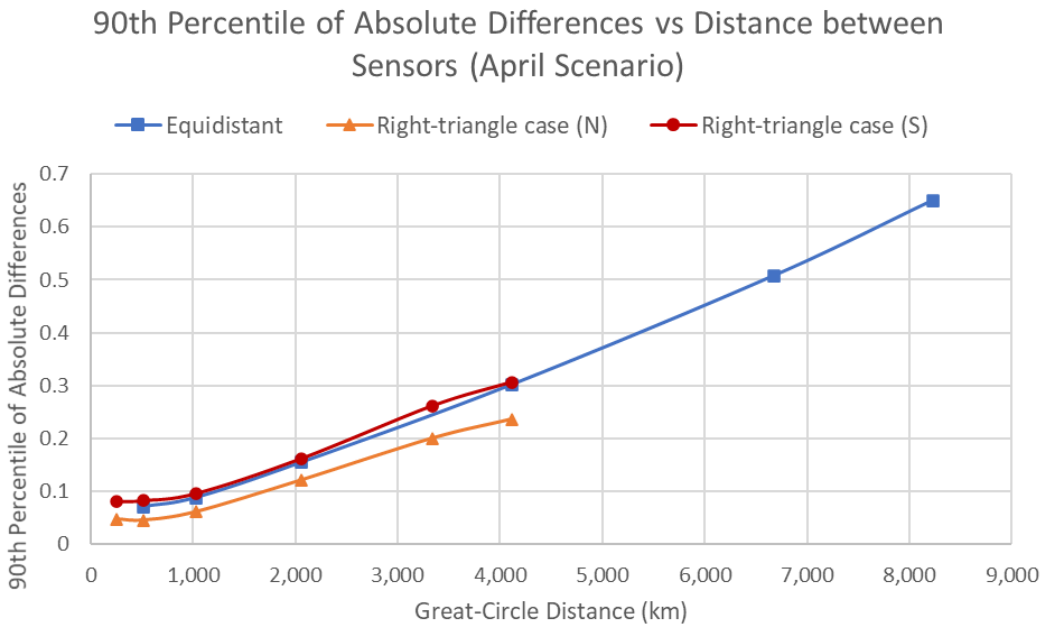

Fig. 21. 90th Percentile of Absolute Magnitude Differences versus North-South Distance (April Scenario)

5. SENSOR FUSION METHOD WITH DISTANCE THRESHOLDS

The process for fusing sensors was updated to incorporate the thresholds determined from our SVST simulations into the pairwise quadratic fitting algorithm. This process is similar to the one described previously that only involves the statistical testing. The addition of distance information between sensors allows us to emphasize the merging of sensors that are closer to one another, over those that are farther away, while still taking into account the p-value from the KS test. Sensor pairs with a distance beyond our established thresholds are prevented from being fused. A description of the algorithm with the distance thresholds incorporated is described next.

5.1 SENSOR FUSION PROCESS

Consider a signature with observations from multiple sensors. Using a quadratic polynomial model, the following procedure is proposed to determine if data from sensor i may be fused with data from sensor j. Let the observations belonging to sensor i be denoted by S_i, i.e., S_i contains all ordered pairs of observations (magnitude and LPA) that belong to the i^{th} sensor. The user-defined significance level for the KS test is $\alpha = 1 \times 10^{-5}$.

For all possible pairs of sensor data in the current signature (i^{th} and j^{th} sensors) and a quadratic model:

1. Fit the model to the datasets S_i and S_j independently by least squares.
2. Calculate the corresponding sets of residuals, R_i and R_j.
3. Fit the model to the combined data $S_{ij} = S_i \cup S_j$ by least squares.
4. Find the residuals for the combined fit R_{ij}.
5. Run the two-sample KS test on $R_i \cup R_j$ and R_{ij}. Report the test's p-value for all sensor pairs.
6. Calculate distance between sensors i and j.
    a. Calculate the great-circle distance between the sensors and label this $distance$.
    b. Calculate the east-west distance between the sensors and label this $distance_{EW}$.
    c. Calculate the north-south distance between the sensors and label this $distance_{NS}$.
7. Iterate through all sensor pairs in order of smallest values of $distance + (1 - p\text{-value})$.
    a. If a sensor pair satisfies $distance_{EW}$ <2500, $distance_{NS}$ <500, and p-value>α, then label that sensor pair i^* and j^*. A high p-value indicates that $R_{i^*} \cup R_{j^*}$ comes from the same distribution as $R_{i^*j^*}$ (i.e., the residuals lack a significant difference in their distributions).

b. Merge the data in S_{i^*} and S_{j^*} if a sensor pair satisfied all requirements.

8. Repeat steps (1) through (7) until the sensors cannot be grouped further.

Once these steps are complete, the grouped sensors from the original signature now form sub-signatures that may be analyzed by characterization or change detection algorithms. The process is repeated for previously grouped sub-signatures that contain multiple sensors; however, a single model is used with sub-signatures containing multiple sensors' data. That is, previously grouped sensors are considered a single sensor from the perspective of the fusion process.

Details are now given about how distance is calculated in the sensor fusion process. Before any sensors are fused, distance can be calculated as the great-circle distance between a pair of sensors. However, after sensors have been fused, distance will need to be calculated between a group of fused sensors and a new sensor (or another group of fused sensors). To handle this situation, distance between a group of fused sensors and a single sensor (or another group of fused sensors) is calculated by taking the maximum distance between each possible sensor pair between fused groups. For example, suppose sensors A and B were fused to create the sensor label AB and sensors C and D were fused to create the sensor label CD. Then to determine if sensor AB should be fused with sensor CD, calculate the distance between sensors A and C, $dist_{AC}$, the distance between sensors A and D, $dist_{AD}$, the distance between sensors B and C, $dist_{BC}$, and the distance between sensors B and D, $dist_{BD}$. The distance between sensor AB and sensor CD is taken to be $\max\{dist_{AC}, dist_{AD}, dist_{BC}, dist_{BD}\}$.

To calculate the east-west distance between a sensor pair, $distance_{EW}$, the distance between the sensors' longitudes is calculated once at the first sensor's latitude and again at the second sensor's latitude then the maximum of those two values is taken as the final estimate of the sensor pair's east-west distance. For example, if sensor A is located at latitude and longitude $(0°, 30°)$ and sensor B is located at $(25°, 100°)$, then the great-circle distance between $(0°, 30°)$ and $(0°, 100°)$ is calculated and the great-circle distance between $(25°, 30°)$ and $(25°, 100°)$ is calculated. The maximum of the two distances calculated is taken as the $distance_{EW}$ for sensors A and B. The north-south distance between a sensor pair, $distance_{NS}$, is calculated by setting the longitudes for the sensors equal and calculating the great-circle distance between their respective latitudes.

5.2 EXAMPLE

To help provide further understanding of this procedure, details of the process are presented to show the intermediate steps that take place for the sensor data shown in Fig. 22. This signature was taken from satellite 38991 on 2019-02-25 and is composed of six different ExoAnalytic Solutions sensors (1141, 1142, 1154, 1176, 1238, and 7012) located in three distinct regions. Each observation is colored by the sensor number. Sensor 7012 is located in US-TX, sensor 1154 is located in US-NM, and sensors 1141, 1142, 1176, and 1238 are located in CL-CO.

Visual inspection reveals two trends in the data, the first being the sensor from US-TX and the second from the sensors in CL-CO and US-NM. However, although the signatures from sensors in CL-CO and US-NM appear to have a similar trend, they have a great-circle distance of about 8000 km. This example will show how the distance thresholds are implemented to prevent the fusion of certain sensor pairs.

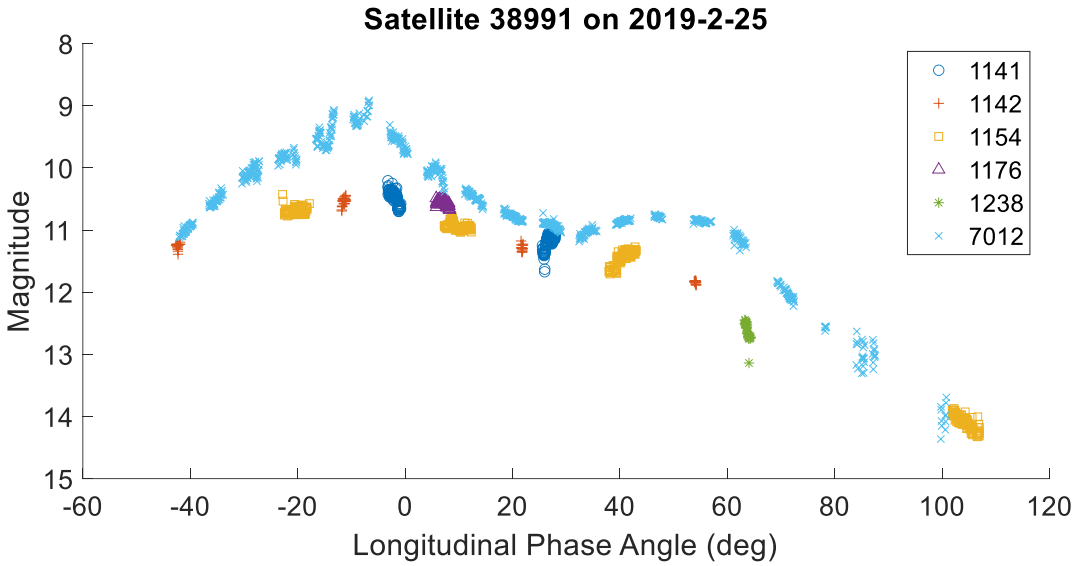

Fig. 22. Signature from Satellite 38991 Taken on 2019-02-25 Where Observations Are Colored by Sensor

For the first run of the algorithm, there are six different sensors contributing data, so $\binom{6}{2} = 15$ pairs of models must be fit by the quadratic function, and their residuals must be analyzed by the KS test. The sensors 1141, 1142, 1154, 1176, 1238, and 7012 are assigned numbers 1-6 respectively in the following plots. For any two of the sensors to be grouped, the p-value reported on residuals from the KS test must be at least $\alpha = 1 \times 10^{-5}$, the great-circle distance between the sensors in the east-west direction must be $\leq$ 2500 km, and the great-circle distance between the sensors in the north-south direction must be $\leq$ 500 km.

Analysis of two of the 15 possible cases for the first iteration are shown in Fig. 23 and Fig. 24. The first case we examine is the sensor grouping $(i, j) = (2,3)$ shown in Fig. 23. Quadratic models were fit to the blue and cyan observations individually, and then a quadratic model was fit to the combined set of blue and cyan observations. The three sets of residuals are shown in the histogram in the bottom of Fig. 23. Based on visual inspection of the histogram, it appears that all of the residuals are highly similar. This indicates a reasonable grouping of these data associated with sensors 2 and 3. The KS test reports a p-value of 0.10 that is well above our grouping threshold of $\alpha = 1 \times 10^{-5}$. However, sensor 2 is located in Chile and sensor 3 is located in the United States so their east-west distance of 3318.18 km and north-south distance of 7046.90 km are above our specified distance thresholds. Therefore, these sensors will not be allowed to fuse at any point due to the distance between them despite the similar trends in their signatures.

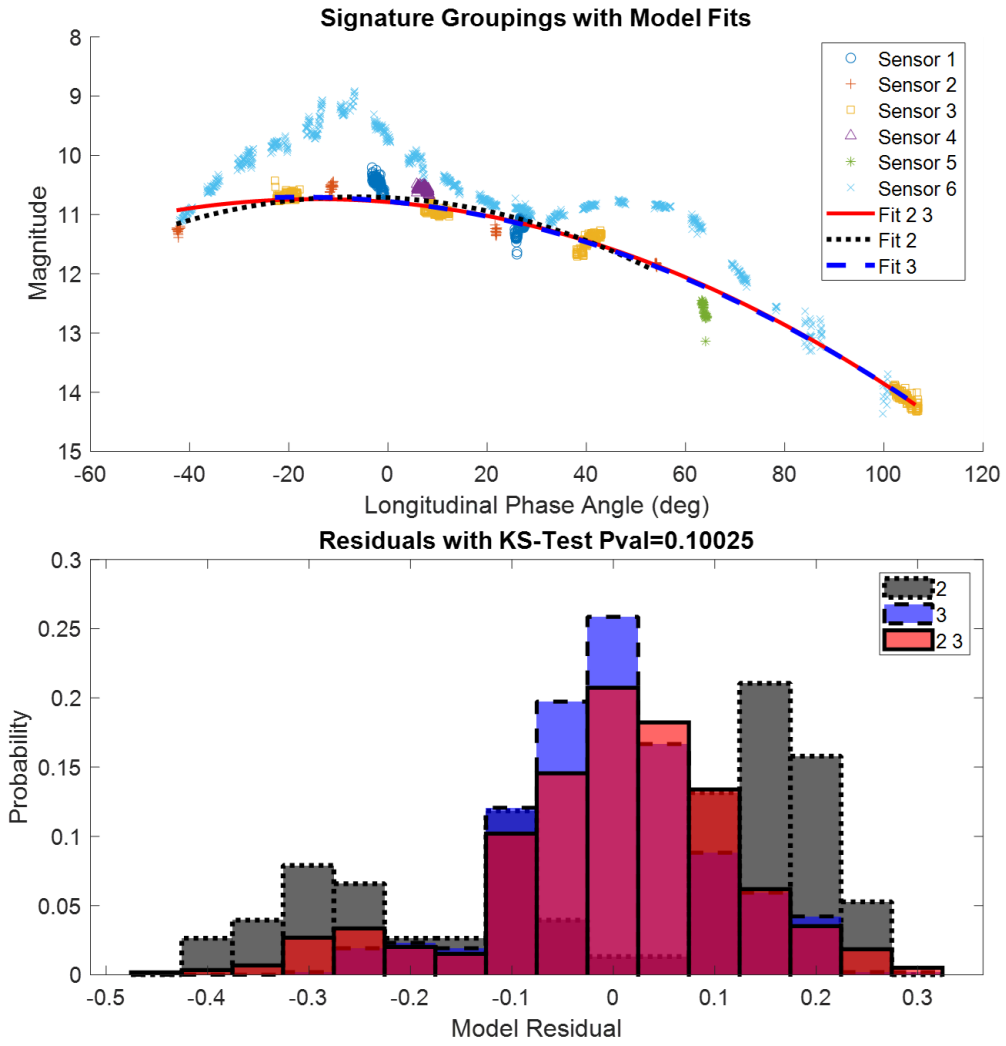

Fig. 23. Signature from Satellite 38991 on 2019-02-25. (Top) Grouping Attempt for Sensor Groups 2 and 3.(Bottom) Residuals from Fits Showing Compatible Residuals

The second case we examine is the sensor grouping $(i, j) = (3,6)$ shown in Fig. 24. Quadratic models were fit to the cyan and dark red observations individually, and then a quadratic model was fit to the combined set of cyan and dark red observations. The three sets of residuals are shown in the histogram at the bottom of Fig. 24. Based on visual inspection of the histogram, it appears that residuals from sensor 3 are highly dissimilar to the residuals from sensor 6 and the residuals from the combined quadratic fit to sensors 3 and 6. This indicates an unreasonable grouping of data associated with sensors 3 and 6. The KS test reports a p-value of 6.83×10^{-23} that is well below our grouping threshold of $\alpha = 1 \times 10^{-5}$. This small p-value will prevent the sensors from being fused in our algorithm even though sensors 3 and 6 come from US-NM and US-TX and their east-west distance of 138.56 km and north-south distance of 257.48 km are well within our distance thresholds.

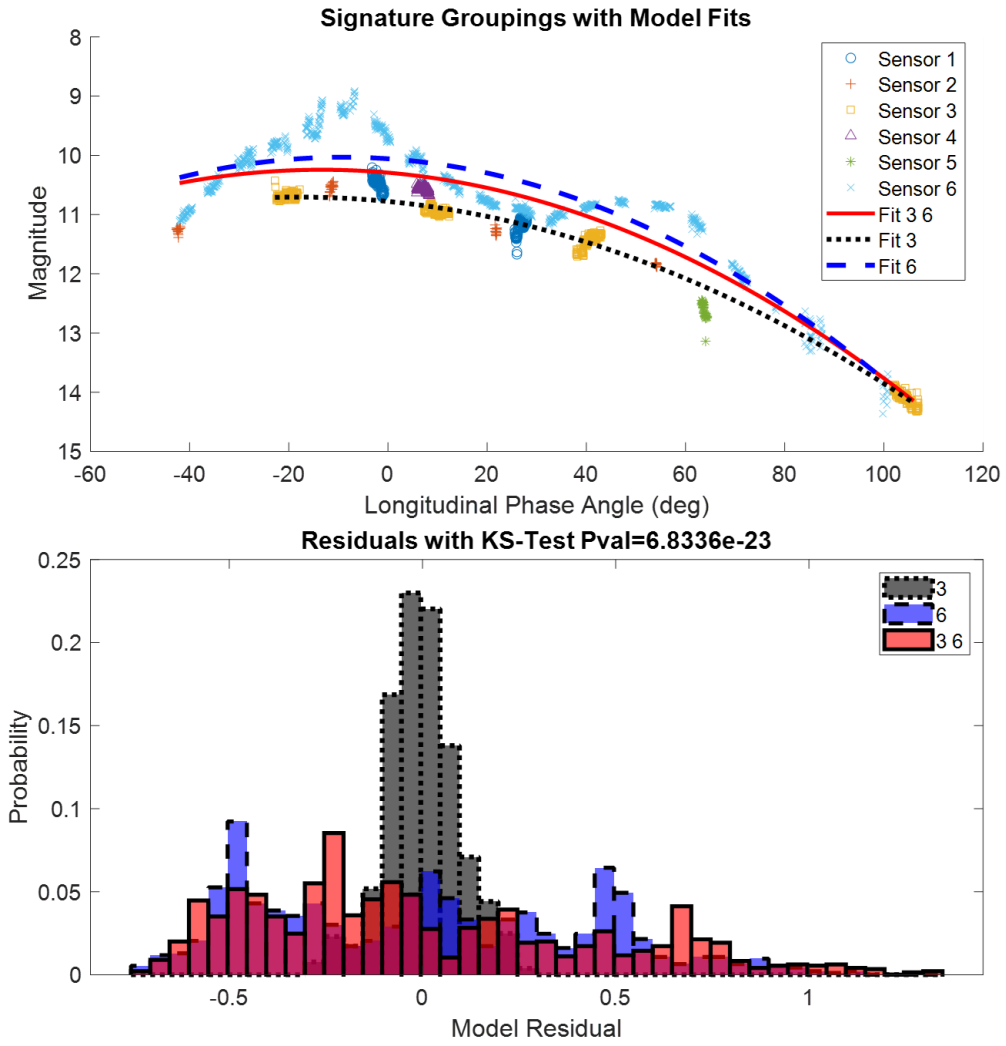

Fig. 24. Signature from Satellite 38991 on 2019-02-25. (Top) Grouping Attempt for Sensor Groups 3 and 6. (Bottom) Residuals from Fits Showing Incompatible Residuals

The p-values and great-circle distances of the remaining sensor pairs tested in the first iteration of the sensor fusion process are reported in Table 4. Since sensor pairs are fused in order of $(distance + (1 - p\text{-value}))$, sensors at the same locations are prioritized. Three sensor pairs have a distance of 0 km, so the sensor pair with 0 km and the largest p-value was fused first, which is sensors 1 and 2. After sensors 1 and 2 are fused, the fused sensor pair will be referred to as sensor 1 in the next iteration of the sensor fusion process.

Table 4. For Signature from Satellite 38991 on 2019-02-25, Reported p-values and Great-Circle Distance for Sensor Groupings from Iteration 1

Grouping Pair	KS Test p-value	Distance (km)
(1,2)	1.7×10^{-3}	0
(1,3)	2.4×10^{-6}	7939.03
(1,4)	2.6×10^{-5}	0
(1,5)	1.9×10^{-3}	37.05
(1,6)	1.1×10^{-9}	7647.81
(2,3)	0.10	7939.03
(2,4)	7.3×10^{-7}	0
(2,5)	0.40	37.05
(2,6)	0.08	7647.81
(3,4)	1.3×10^{-4}	7939.03
(3,5)	0.21	7911.03
(3,6)	6.8×10^{-23}	291.59
(4,5)	0.08	37.05
(4,6)	9.5×10^{-5}	7647.81
(5,6)	0.3	7619.88

After combining sensors 1 and 2 together (now referred to as label 1), we are left with five groupings to analyze pairwise. This results in $\binom{5}{2} = 10$ pairwise tests to run. The p-values for these ten pairwise KS tests and the corresponding great-circle distances are in Table 5. The values indicate that sensor groups 1 and 4 may be combined (to be labeled as group 1) because they have the smallest distance 0 km and a p-value above our threshold of $\alpha = 1 \times 10^{-5}$.

Table 5. For Signature from Satellite 38991 on 2019-02-25, Reported p-values and Great-Circle Distance for Sensor Groupings from Iteration 2

Grouping Pair	KS Test p-value	Distance (km)
(1,3)	0.15	7939.03
(1,4)	7.8×10^{-4}	0
(1,5)	0.50	37.05
(1,6)	1.5×10^{-8}	7647.81
(3,4)	1.3×10^{-4}	7939.03
(3,5)	0.21	7911.03
(3,6)	6.8×10^{-23}	291.59
(4,5)	0.08	37.05
(4,6)	9.5×10^{-5}	7647.81
(5,6)	0.03	7619.88

For the third run of the algorithm, there are now only four sensor groupings remaining. This results in $\binom{4}{2} = 6$ pairs whose p-values and great-circle distances are given in Table 6. The sensor groupings labeled 1 and 5 have the smallest distance of 37.05 km and a p-value of 0.08 from the KS test which is larger than our threshold of $\alpha = 1 \times 10^{-5}$; thus, these are grouped together and labeled 1.

Table 6. For Signature from Satellite 38991 on 2019-02-25, Reported p-values and Great-Circle Distance for Sensor Groupings from Iteration 3

Grouping Pair	KS Test p-value	Distance (km)
(1,3)	9.1×10^{-6}	7939.03
(1,5)	0.08	37.05
(1,6)	6.2×10^{-16}	7647.81
(3,5)	0.21	7911.03
(3,6)	6.8×10^{-23}	291.59
(5,6)	0.03	7619.88

In the final run of the algorithm, there are three sensor groupings remaining. This results in $\binom{3}{2} = 3$ pairs of tests whose p-values and great-circle distances are given in Table 7. Only sensors 3 and 6 from US-NM and US-TX are within the distance threshold; however, the p-value for this sensor pair is well below the chosen significance level for the KS test, $\alpha = 1 \times 10^{-5}$.

Table 7. For Signature from Satellite 38991 on 2019-02-25, Reported p-values and Great-Circle Distance for Sensor Groupings from Iteration 4

Grouping Pair	KS Test p-value	Distance (km)
(1,3)	1.3×10^{-6}	7939.03
(1,6)	3.8×10^{-17}	7647.81
(3,6)	6.8×10^{-23}	291.59

Since none of the three sensor pairs are eligible for fusion, the sensor fusion process ends with three sub-signatures, as shown in Fig. 25. The final sensor groupings correspond to the three distinct regions in which the sensors are located. In Fig. 25, sensor grouping 1 plotted as blue circles corresponds to all sensors located in CL-CO. Sensor grouping 2 plotted as orange plus signs corresponds to the sensor located in US-NM, and sensor grouping 3 plotted as yellow squares corresponds to the sensor located in US-TX.

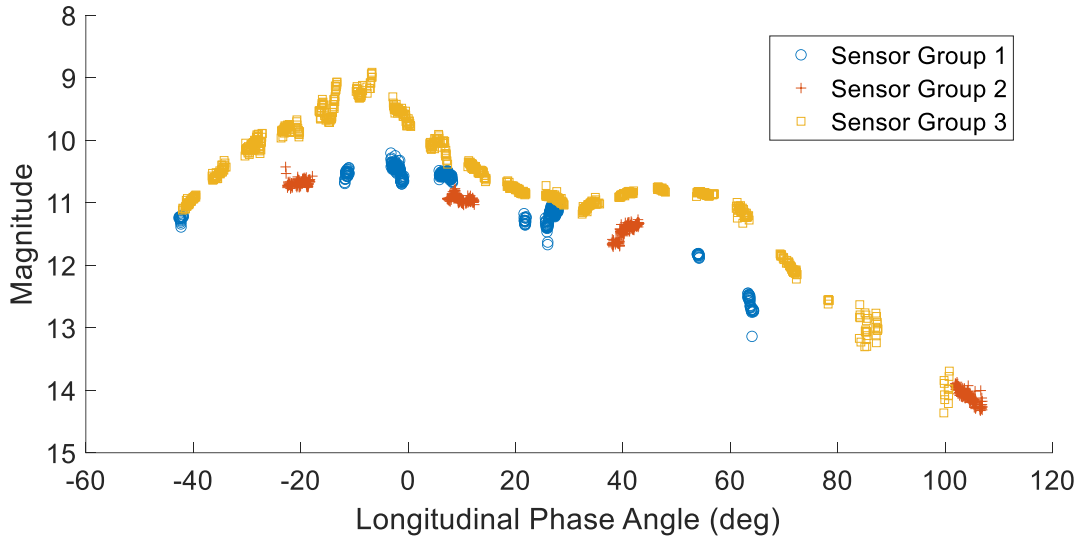

Fig. 25. Multi-sensor Data from Satellite 38991 on 2019-02-25 (Shown in Fig. 22) Grouped Based on Great-Circle Distance and Residuals from Fits to Pairs of Sensors

6. RESULTS

To further test our algorithm, we identified several more multi-sensor signatures and performed sensor fusion with our combined algorithm that takes both data trends and sensor locations into account. The results of the sensor fusion process on three of these multi-sensor signatures are shown in this section.

The first example comes from satellite 25894 on 2019-02-08. This signature is plotted in Fig. 26 where observations are labeled by the sensor number. Seven sensors from four distinct regions of Australia contributed to this multi-sensor signature. Sensors 1174 and 1175 are located in AU-SA, sensors 1233, 1234, and 1299 are located in AU-WA, sensor 1276 is located in AU-NT, and sensor 7007 is located in AU-VIC.

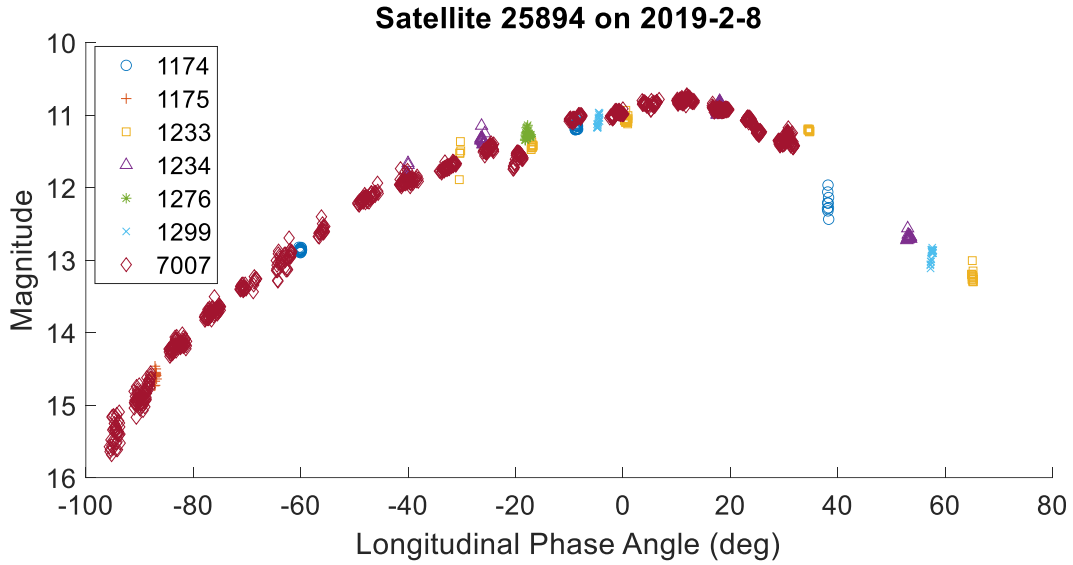

Fig. 26. Signature from Satellite 25894 Taken on 2019-02-08

The observations from all of the sensors appear to follow generally the same trend which would make them all candidates for fusion, but the distance between sensors in different regions of Australia prevents all sensors from being fused. The final groupings for these sensors are given in Table 8 and plotted in Fig. 27. Group 1 contains all sensors from AU-SA and the sensor from AU-VIC. Group 2 contains all sensors in AU-WA and group 3 contains the sensor in AU-NT. All sensors within range of one another were fused, so the final groups cannot be further fused due to the distance in the east-west direction, north-south direction, or both directions surpassing the set thresholds. As a result, most groupings correspond to the region in which each sensor is located. These results are reasonable since sensors in the same region will see the same view of the satellite which is supported by the signatures from each sensor having similar trends.

Table 8. Sensor Number, Location, and Grouping for Sensor Fusion Performed on Signature from Satellite 25894 on 2019-02-08

Sensor Number	Location	Group
1174	AU-SA	1
1175	AU-SA	1
1233	AU-WA	2
1234	AU-WA	2
1276	AU-NT	3
1299	AU-WA	2
7007	AU-VIC	1

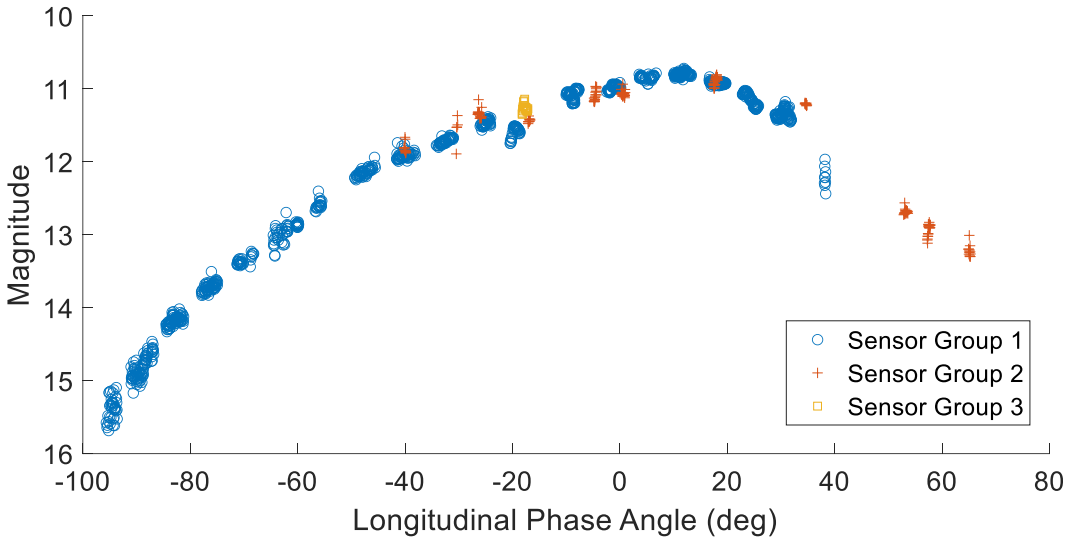

Fig. 27. Multi-sensor Data from Satellite 25894 on 2019-02-08 (Shown in Fig. 26) Grouped Based on Great-Circle Distance and Residuals from Fits to Pairs of Sensors

The second example comes from satellite 43874 on 2019-01-03. This signature is plotted in Fig. 28 where observations are labled by the sensor number. Eleven sensors from four distinct regions contributed to this multi-sensor signature. Sensor 1219 is located in ZA-NC, sensors 1260 and 1262 are located in AU-WA, sensors 1284, 1312, 1313, 1320, and 7028 are located in GR-M, and sensors 1309, 1314, and 1317 are located in ZA-WC.

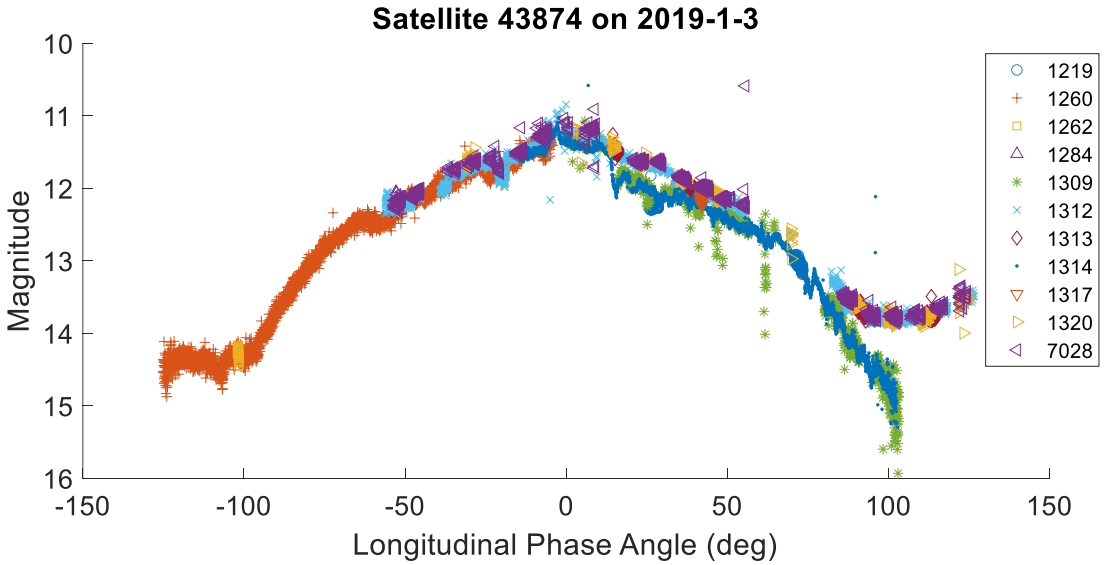

Fig. 28. Signature from Satellite 43874 Taken on 2019-01-03

The observations from all of the sensors overlap near the peak at 0° LPA but differ on the ends of the signature. One area where the differing trends is visually evident is around 100° LPA where one trend (mostly plotted as blue dots) decreases in brightness while the other (mostly plotted as purple left-pointing triangles) increases. Ideally these different trends will be fused into separate groups.

The final groupings for the signature from satellite 43874 taken on 2019-01-03 are given in Table 9 and plotted in Fig. 29. Group 1 consists of the one sensor located in ZA-NC. Group 2 contains the sensors in AU-WA. Group 3 contains all sensors in GR-M, and group 4 contains all sensors in ZA-WC. All sensors within range of one another were fused, so the final groups cannot be further fused due to the distance between sensor pairs.

Though the sensors from different regions of South Africa (ZA-NC and ZA-WC) appear to have similar trends (as seen in Fig. 29 plotted as blue circles and purple triangles), they cannot be fused due to the north-south distance between them being just above our threshold of 500 km. As a result, each of the final groupings correspond to the distinct regions in which these sensors are located. These results are reasonable since sensors in South Africa, Greece, and Australia all have visually different trends from one another and their distances are well above our thresholds.

Table 9. Sensor Number, Location, and Grouping for Sensor Fusion Performed on Signature from Satellite 43874 on 2019-01-03

Sensor Number	Location	Group
1219	ZA-NC	1
1260	AU-WA	2
1262	AU-WA	2
1284	GR-M	3
1309	ZA-WC	4
1312	GR-M	3
1313	GR-M	3
1314	ZA-WC	4
1317	ZA-WC	4
1320	GR-M	3
7028	GR-M	3

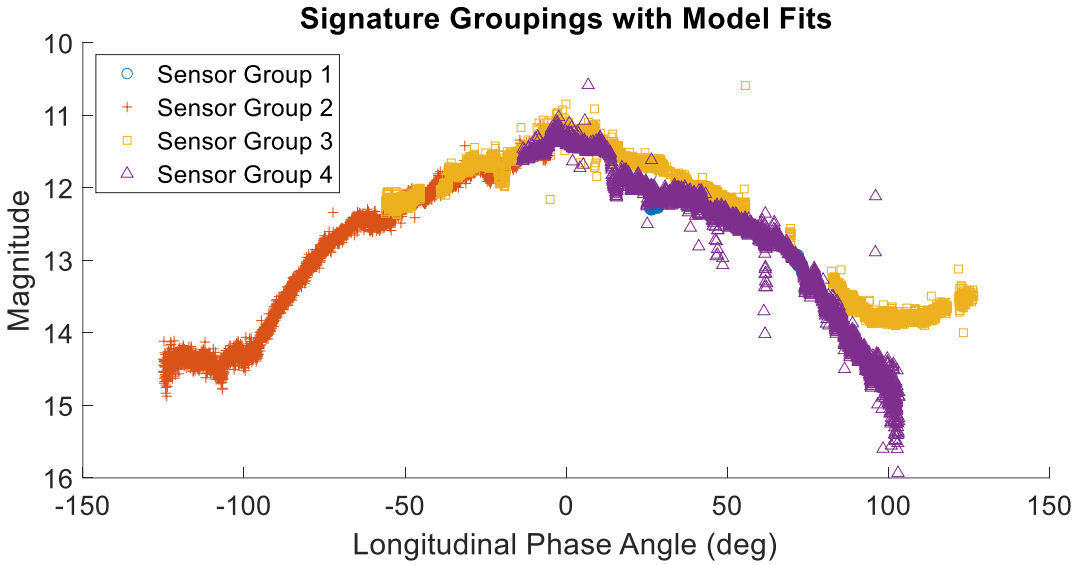

Fig. 29. Multi-sensor Data from Satellite 43874 on 2019-01-03 (Shown in Fig. 28) Grouped Based on Great-Circle Distance and Residuals from Fits to Pairs of Sensors

The final example comes from satellite 38991 on 2019-01-04. This signature is plotted in Fig. 30 where observations are colored by the sensor number. Nine sensors from four distinct regions contributed to this multi-sensor signature. Sensor 1047 is located in US-CA, sensor 1154 is located in US-NM, sensor 7012 is located in US-TX, and sensors 1141, 1142, 1145, 1186, 1189, and 1191 are located in CL-CO. Visually, the data from sensors in US-TX and US-CA appear similar (orange downward-pointing triangles and blue circles) while the data from the sensor in US-NM (green asterisks) appears more similar to the data from sensors located in CL-CO (red diamonds, light blue x's, etc.). From visual inspection alone, it seems reasonable that sensors in US-CA and US-TX would be fused, while the US-NM sensor will be unable to fuse with the other US sensors due to its signature trend and unable to fuse with CL-CO sensors due to the distance.

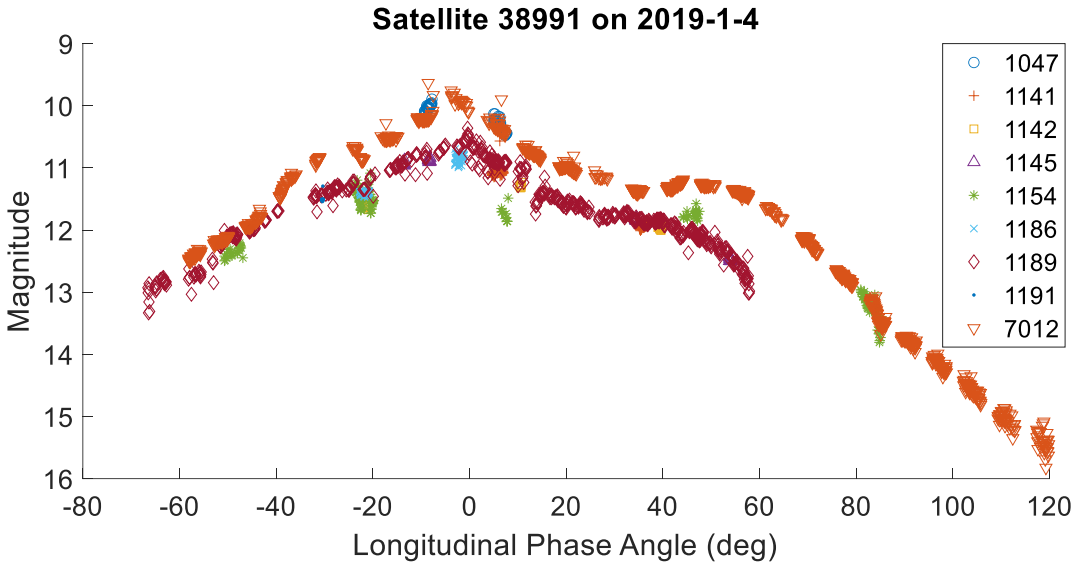

Fig. 30. Signature from Satellite 38991 Taken on 2019-01-04

The final groupings for the signature from satellite 38991 taken on 2019-01-04 are given in Table 10 and plotted in Fig. 31. Group 1 consists of the one sensor located in US-CA. Group 2 contains all sensors in CL-CO. Group 3 contains the sensors in US-TX and US-NM. All sensors within range of one another were fused, so the final groups cannot be further fused due to the distance between sensor pairs. Though the sensors in US-CA and US-TX have similar trends, their north-south distance is about 720 km which is above our threshold of 500 km. Alternatively, though US-TX and US-NM do not have similar trends throughout the center of the signature around $[-20°, 60°]$ LPA, they were grouped by the sensor fusion process.

This unexpected grouping of US-TX and US-NM may be the result of using a simple quadratic model which resulted in a good fit at the ends of the signatures but a poor fit to the center of the signatures for both sensors. Due to this poor fit, the residuals for the two sensors' signatures were similar enough for the KS test to determine that their residuals came from the same distribution (which resulted in their grouping). It is possible that trying a different model could change the results for this signature.

Table 10. Sensor Number, Location, and Grouping for Sensor Fusion Performed on Signature from Satellite 38991 on 2019-01-04

Sensor Number	Location	Group
1047	US-CA	1
1141	CL-CO	2
1142	CL-CO	2
1145	CL-CO	2
1154	US-NM	3
1186	CL-CO	2
1189	CL-CO	2
1191	CL-CO	2
7012	US-TX	3

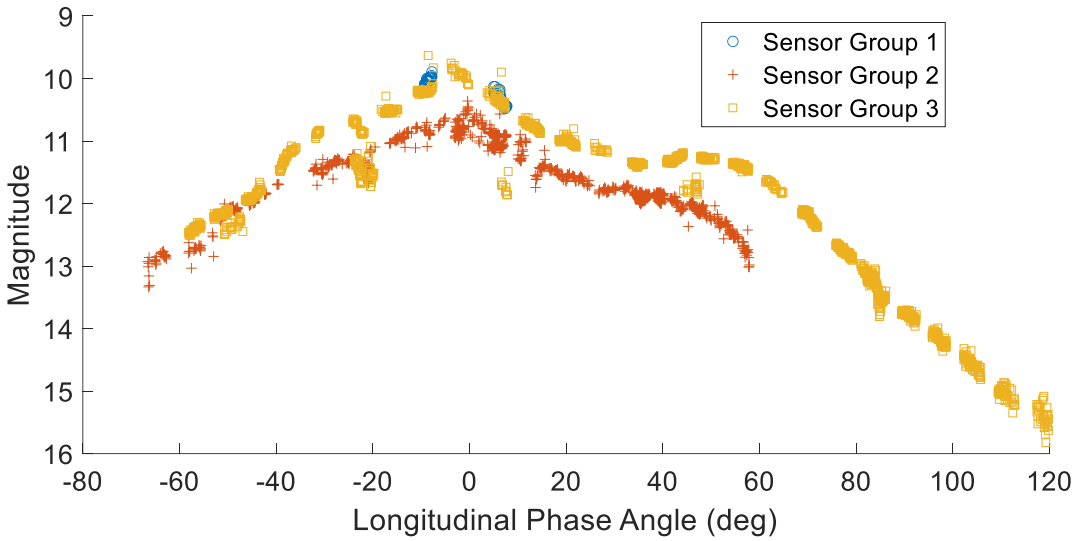

Fig. 31. Multi-sensor Data from Satellite 38991 on 2019-01-04 (Shown in Fig. 30) Grouped Based on Great-Circle Distance and Residuals from Fits to Pairs of Sensors

7. CONCLUSIONS

For the examples tested, the algorithm we developed to fuse sensors at different sites matches our expectations. Generally, sensors are grouped by our empirically-derived geographic constraints, which is necessary due to viewing angle differences. In most of the examples, the geographic constraints yielded acceptable results, i.e., the sensors' signatures followed the same trend. However, there were notable exceptions. The results on the signature from satellite 38991 taken on 2019-01-04 provides an example where the algorithm fused two sensors based on distance despite their brightness trends differing throughout a large portion of the night.

We found that significant offsets between sensors exist in the UDL data set even though they met our "closeness" criteria and they belong to the same commercial provider. There are at least two possible causes. These offsets could be caused by using different photometric systems to transform the photometry to a standard magnitude system and/or the offsets could be caused by inaccurate atmospheric removal. An example of the latter is using extinction coefficients from a different night or a zero-point value from a different site. Therefore, one of our conclusions is that it would be beneficial to Space Domain Awareness (SDA) if we, as a community, could standardize the calibration process and decide on one photometric system to use for satellite photometry (see [5]).

With some further testing and updates, this algorithm could be used to automatically group sensor data for nights that multiple sensors observe the same satellite. This would help make the large amount of data accessible through UDL more useful as fusing data provides signatures with more data points covering larger ranges of LPA for the entire night. Additionally, the algorithm's ability to prevent certain sensors from being fused will help avoid errors when the signatures containing dissimilar information are run through characterization and change detection algorithms. The automation of the process means more data can be processed quickly, which is crucial given the amount of commercial data available through the UDL.

8. FUTURE WORK

Certain aspects of the sensor fusion algorithm were chosen based on performance on a handful of examples. The algorithm could be further improved by optimizing settings including the model used to fit data from sensor pairs and the significance level used in the KS test.

A quadratic model was used initially due to its simplicity so as to not overfit any one sensor's signature and because the general shape of a stable three-axis-stabilized GEO satellite's signature is a parabola (i.e., dim for observations away from 0° LPA and bright near 0° LPA). A higher degree polynomial may help prevent sensors from being fused due to a poor fit to the data. The ideal degree of the polynomial model could be chosen through cross-validation

techniques run on a per sensor basis. The higher degree chosen for a sensor pair could then be used to fit the union of data from a sensor pair.

The significance level, α, for the KS test could also be improved by further testing the algorithm on a larger set of data. For instance, ideal sensor groupings could be identified manually, and α could be optimized such that the largest number of ideal groupings occur.

We plan to extend this approach for data collected on cislunar objects since their orbits are such that their brightness trends sample a larger range of viewing geometries. This future work will entail higher dimensional analysis. Additionally, our test for identifying similar brightness trends is data agnostic and applicable to cislunar object brightness data.

9. ACKNOWLEDGEMENTS

The authors would like to thank Air Force Research Laboratory (AFRL) for sustaining the UDL program that has allowed us to explore multi-site, multi-sensor data fusion for SDA. We would also like to thank ExoAnalytic Solutions for its data. We would also like to thank AFRL for SVST (a vital tool in our analysis) and Dr. Gregg Crockett at Tau Technologies for his timely answers to our various questions using SVST for this research.

REFERENCES

[1] S. Erwin, "Bluestaq wins $280 million Space Force contract to expand space data catalog," Pocket Ventures LLC, 23 March 2021. [Online].

[2] BlueStaq, [Online]. Available: https://unifieddatalibrary.com/. [Accessed June 2021].

[3] F. J. Massey, "The Kolmogorov-Smirnov Test for Goodness of Fit," *Journal of the American Statistical Association,* vol. 46, no. 253, pp. 68-78, 1951.

[4] G. A. Crockett and R. L. Brunsun, "Visualization tool for advanced laser system development," *SPIE Proceedings: Laser Weapens Technology III,* vol. 4724, 25 June 2002.

[5] P. Castro, T. Payne, K. Kinateder and T. Godar, "Calculating Photometric Uncertainty," in *AMOS Conference Proceedings*, Wailea, 2020.